Border Collision Bifurcations of Stroboscopic Maps in Periodically Driven Spiking Models[*]

A. Granados[†], M. Krupa[†], and F. Clément[†]

Abstract. In this work we consider a general nonautonomous hybrid system based on the integrate-and-fire model, widely used as simplified version of neuronal models and other types of excitable systems. Our assumptions are that the system is monotonic, possesses an attracting subthreshold equilibrium point, and is forced by means of a periodic pulsatile (square wave) function. In contrast to classical methods, in our approach we use the stroboscopic map (time-T return map) instead of the so-called firing map. It becomes a discontinuous map potentially defined in an infinite number of partitions. By applying theory for piecewise-smooth systems, we avoid relying on particular computations, and we develop a novel approach that can be easily extended to systems with other topologies (expansive dynamics) and higher dimensions. More precisely, we rigorously study the bifurcation structure in the two-dimensional parameter space formed by the amplitude of the pulse and the ratio between T and the duration of the pulse (duty cycle). We show that it is covered by regions of existence of periodic orbits given by period adding structures. The period adding structures completely describe not only all the possible spiking asymptotic dynamics but also the behavior of the firing rate, which is a devil's staircase as a function of the parameters.

1. Introduction. In the context of neuronal modeling (and similarly for hormone release), one relies on systems that are able to exhibit large-amplitude responses under certain stimuli. An example of such behavior is an *action potential* (AP) or *spike* of a neuron. There exist accurate but quite complex models of APs, e.g., the Hudgkin–Huxley equations [HH52]. Simpler models are the Morris–Lecar [ML81] or the FitzHugh and Nagumo [Fit61, NAY62]. All these models use the principle of excitability and often exhibit slow–fast dynamics.

Hybrid systems with resets are used as approximate models of excitability, with the discontinuity, that is, the reset, used to mimic the spike. In many contexts, a spike occurs when the system receives a sufficient amount of stimulus.

One can distinguish between different types of systems with resets. The simplest are *integrate-and-fire* models, for which the differential equation exhibits very simple dynamics (it is constant or linear). Other models include more complicated subthreshold dynamics

including instabilities (which introduce expanding dynamics) in order to provide more realistic representations of the underlying phenomena. This is the case of the so-called Izhikevich model [Izh03]. Other approaches [BG05, TB09, MHR12] let the threshold depend on the state variable (thus increasing the dimension of the system) in order to obtain a more accurate model with possibly more complex properties, as is the case of type III neurons [CPF08, Izh07].

Due to the discontinuity in the trajectories given by the reset, one cannot directly apply classical theory for smooth systems in order to study these types of excitable systems. A typical approach to overcoming this problem is to consider the so-called *adaptation*, *firing*, or *impact* map, which is a Poincaré map onto the threshold [KHR81, CB99, CTW12, TB09, JMB$^+$13, DKTG12]; that is, one takes an initial condition on the threshold (which leads to a reset) and one then integrates the system until the threshold is reached again. This is a well-known technique also in other disciplines involving piecewise-smooth dynamics (see [dBBCK08] for examples); this map becomes the composition of smooth maps and hence provides a regular version of the system which can be studied by means of classical tools for smooth systems.

Note that, in order to compute the firing map, one needs to know the time needed by the system to perform the next spike (firing times). Even assuming linearity, these times need to be computed numerically, as they involve transcendental equations. Hence, one also relies on numerical computations in order to derive properties of the firing map.

When introducing a T-periodic forcing to the system (a periodic current in the neuronal context), the firing map must include time as a variable. In fact, for the one-dimensional case, it becomes a map that returns the next firing time. Hence, in order to study the existence of periodic orbits, explicit knowledge of the behavior of these times becomes crucial, as one needs to check whether the difference between consecutive spiking times is congruent (rational multiple) with T. Results in the context of firing maps have been obtained in specific cases. For example, it was shown in [KHR81] that, for a linear system, by using the explicit expression for the flow, one can approximate the firing map by a certain circle map and derive information about rotation and firing numbers of existing periodic orbits. By combining this same technique with numerical simulations, it was shown in [COS01] that one obtains similar results when introducing a periodic forcing to a two-dimensional integrate-and-fire-or-bursting system. There the authors studied in more detail the existence of periodic orbits (mode locking) and showed numerically that the firing number may follow a devil's staircase as a function of parameters.

In this work we present a new approach to studying periodically forced systems with resets based on the use of the so-called stroboscopic map (time-T return map). One of the advantages of our approach is that it leads to a general setting for periodically forced systems. Already in the smooth case such systems are better understood by means of the stroboscopic map than with Poincaré maps onto transverse sections in the state space. In the latter, as mentioned above, one has to check for congruency between the passage times and the period of the forcing, which requires explicit knowledge of the solutions of the system or approximations by circle maps in order to study the existence of periodic orbits. However, when dealing with the stroboscopic map, this is reduced to the study of existence of fixed (or periodic) points of this map, which comes by applications of classical results as the implicit function theorem (when studying perturbations) or Brouwer's theorem.

The use of the stroboscopic map has been avoided in systems with resets because it

becomes a discontinuous (piecewise-smooth) map. The sets of initial conditions for which this map becomes smooth are identified by the number of spikes exhibited by their trajectories when flowed for a time T, and hence this map is potentially defined in an arbitrarily large number of partitions. However, in this work we use recent results in nonsmooth systems to face these discontinuities and rigorously study a general and large class of hybrid systems with resets.

More precisely, we consider a one-dimensional monotonic system with an attracting sub-threshold equilibrium point under a T-periodic forcing consisting of a periodic square wave function. This is given by a pulse of amplitude A and duration dT, with $0 \leq d \leq 1$ (duty cycle), and is 0 for the rest of the period T. Such a periodic stimulus is used in many contexts, as the stimulation of an excitable cell (e.g., a hormone release) frequently occurs in a pulsatile form. Such a periodic forcing indeed adds an extra nonsmoothness, as one switches from one autonomous system to another at the switching times, when the pulse is switched on or off. However, this singularity consists of a discontinuity on the field that neither adds nor removes extra dynamical objects and bifurcations. As usual when dealing with piecewise-smooth fields, in this case the solutions of the system are continuous and obtained by proper concatenation of the solutions of both fields, as long as the threshold is not reached.

Our results consist of a rigorous and detailed description of the bifurcation scenario formed by the parameters describing the input pulse: its amplitude A and its duty cycle d. We show that there exists an infinite number of regions in this two-dimensional parameter space for which the stroboscopic map exhibits a fixed point. The regions in between are covered by regions of existence of periodic orbits following the so-called period adding structure. The rotation number associated with these periodic orbits is a devil's staircase as a function of the parameters. This allows us to show that the asymptotic firing rate of the system also follows a devil's staircase when the mentioned parameters are varied.

This work is organized as follows.

In section 2 we describe the system, announce our results, and describe the state of the art in piecewise-smooth maps relevant to our work. In section 3 we prove our results, and in section 4 we validate them by providing numerical computations for three examples.

2. Background and results. Let us consider a nonautonomous periodic system given by

$$(2.1) \qquad \dot{x} = f(x) + I(t), \quad x \in \mathbb{R},$$

with $f(x) \in C^\infty(\mathbb{R})$ and $I(t)$ a T-periodic square-wave function

$$(2.2) \qquad I(t) = \begin{cases} A & \text{if } t \in (nT, nT + dT)], \\ 0 & \text{if } t \in (nT + dT, (n+1)T], \end{cases}$$

with $0 \leq d \leq 1$. Let us submit system (2.1) to the reset condition

$$(2.3) \qquad x = \theta \longrightarrow x = 0;$$

that is, the trajectories of system (2.1) are instantaneously reset to 0 whenever they reach the threshold given by $x = \theta$. This provides a new system which is in the class of *hybrid* systems, as it combines an algebraic condition with a differential equation. Due to the generality

of function f, this system represents a large class of the *spiking* models which are used as simplifications of slow–fast systems modeling excitable cells as neurons. Hence, we will refer to the discontinuities given by the reset condition as spikes.

Let us assume that the system

$$\dot{x} = f(x) \tag{2.4}$$

satisfies the following conditions:

H.1. It possesses an attracting equilibrium point

$$0 < \bar{x} < \theta. \tag{2.5}$$

H.2. $f(x)$ is a monotonic decreasing function in $[0, \theta]$:

$$f'(x) < 0, \quad 0 \le x \le \theta.$$

The reset condition (2.3), in combination with conditions H.1–H.2, implies that the dynamics we are interested in is located in the interval $[0, \theta)$. In fact, by identifying $0 \sim \theta$, this interval can be seen as a circle. However, for our convenience, from now on we will consider the state space to be given by the interval $[0, \theta)$.

Note that the fact that the equilibrium point $\bar{x}$ is globally attracting in $[0, \theta)$ prevents the system from exhibiting spikes without the input. It can hence be considered as the limit of a slow–fast system.

One of the most relevant features of the asymptotic dynamics of system (2.1)–(2.3) is the *firing rate*, i.e., the average number of spikes exhibited by the system per unit time:

$$r(x_0) = \lim_{\tau \to \infty} \frac{\#(\text{spikes performed by } \phi(t; x_0) \text{ for } t \in [0, \tau])}{\tau}, \tag{2.6}$$

where $\phi(t; x_0)$ is the trajectory of the system with $\phi(0; x_0) = x_0$. When the system possesses an attracting periodic orbit, this quantity does not depend on the initial condition x_0 and becomes the number of spikes performed by this periodic orbit along one period divided by the length of the period.

Hence, to obtain a qualitative and quantitative description of the firing rate we study the existence of periodic orbits for system (2.1)–(2.3) and their bifurcations under conditions H.1–H.2. In particular, we provide a full description of the bifurcation scenario for the two-dimensional $(d, 1/A)$-parameter space, which is shown in Figure 1. More precisely, under conditions H.1–H.2 and for any $T > 0$, we prove the following.

- The $(d, 1/A)$-parameter space, $d \in (0, 1)$, contains an infinite number of disjoint bounded regions (gray regions in Figure 1(a)) for which system (2.1)–(2.3) possesses a unique globally attracting T-periodic orbit (fixed point of the stroboscopic map). These regions are ordered clockwise in such a way that the T-periodic orbit corresponding to the next region exhibits one spike more per period than the previous one (Propositions 3.2 and 3.3).

- In between the regions corresponding to the existence of fixed points of the stroboscopic map (gray regions) are the regions defined by the existence of periodic orbits of arbitrarily large periods (white regions). These periodic orbits are organized by the period adding structure (Proposition 3.4).
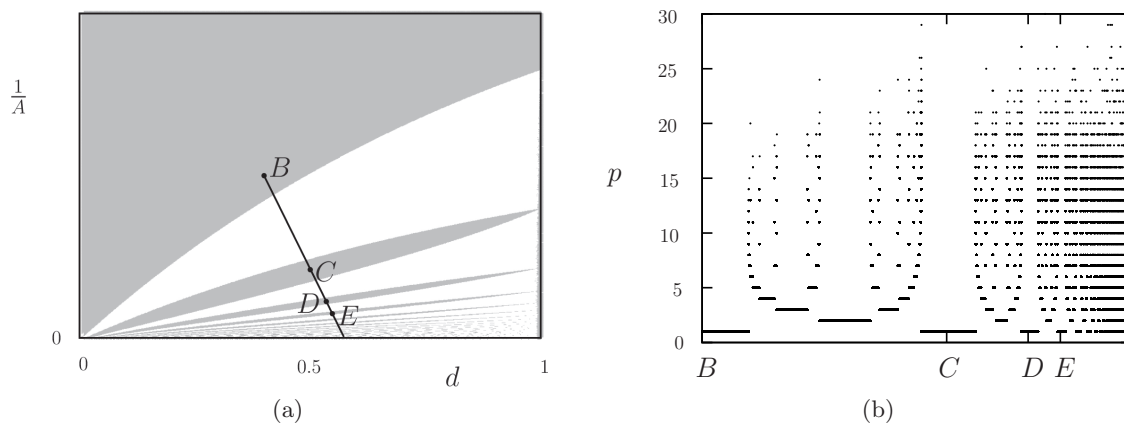
Figure 1. (a) *Bifurcation scenario for system* (2.1)–(2.3). *In gray regions there exist T-periodic orbits, and in white regions there exist higher periodic orbits following an adding structure (see text). In B, C, D, and E one finds T-periodic orbits spiking 0, 1, 2, and 3 times per period, respectively.* (b) *Periods of the periodic orbits found along the line shown in* (a).

- Along any invertible and continuous curve

$$\lambda \in \mathbb{R} \longmapsto (d(\lambda), 1/A(\lambda))$$

satisfying $d(\lambda) \in (0,1)$, $(1/A(\lambda))' < 0$, $1/A(\lambda) \to 0$ when $\lambda \to \infty$ and crossing all the regions mentioned above (as the straight line labeled in Figure 1(a)), the firing rate evolves following a devil's staircase from 0 to ∞. This is explained in section 3.4 and is a consequence of Proposition 3.4.

The main tool that we will use to prove the previous results is the stroboscopic map at return time T. As will be shown, this is a piecewise-smooth map defined on an infinite number of domains containing initial conditions for which system (2.1)–(2.3) exhibits different numbers of spikes when flowed for a time T. For each domain, there exist parameter values d and A for which this map has a fixed point located in this domain; these parameter values correspond to the gray regions in Figure 1.

Between two consecutive regions where fixed points exist (white regions in Figure 1(a)), the stroboscopic map is discontinuous at the boundary between two consecutive domains and can be written as the normal form map

$$(2.7) \qquad g(x) = \begin{cases} \mu_{\mathcal{L}} + g_{\mathcal{L}}(x) & \text{if } x < 0, \\ -\mu_{\mathcal{R}} + g_{\mathcal{R}}(x) & \text{if } x > 0, \end{cases}$$

with $g_{\mathcal{L}}, g_{\mathcal{R}}$ smooth functions satisfying $g_{\mathcal{L}}(0) = g_{\mathcal{R}}(0) = 0$. As the stroboscopic map is given by the integration of a flow, its fixed points have positive associated eigenvalues, and hence $g_{\mathcal{L}}(x)$ and $g_{\mathcal{R}}(x)$ are increasing functions near the origin. Moreover, due to the assumption $f' < 0$, the stroboscopic map is everywhere contracting (under the conditions of Lemma 3.4), so that $|g_{\mathcal{L}}'| < 1$ and $|g_{\mathcal{R}}'| < 1$.
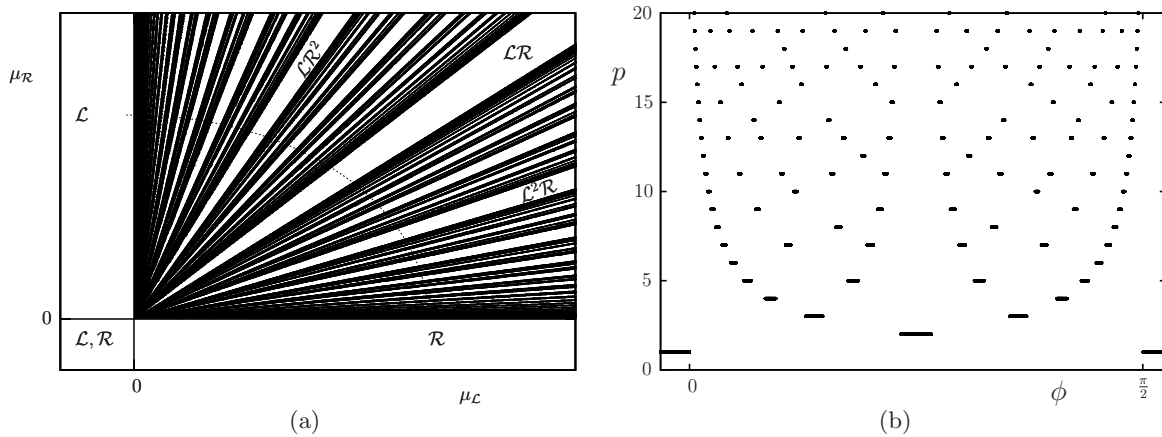
Figure 2. *The period adding big bang or gluing bifurcation.* (a) $(\mu_{\mathcal{L}}, \mu_{\mathcal{R}})$-*parameter space;* (b) *periods of the periodic orbits along the curve shown in* (a).

We first describe the bifurcation scenario for map (2.7), which is shown in Figure 2. The following statements are not obvious and partially come from results scattered throughout the literature (see references below). They have been recently assembled and completed in a review article [GAK14].

Note that, for $|\mu_{\mathcal{L}}|, |\mu_{\mathcal{R}}|$ small enough, if $\mu_{\mathcal{L}} < 0$ and $\mu_{\mathcal{R}} < 0$, the map (2.7) possesses two fixed points, each at each side of the boundary $x = 0$, which undergo border collision bifurcations when $\mu_{\mathcal{L}} = 0$ and $\mu_{\mathcal{R}} = 0$, respectively. Hence, for $\mu_{\mathcal{L}} = \mu_{\mathcal{R}} = 0$ both fixed points simultaneously collide with the boundary, undergo border collision bifurcations, and no longer exist. For $\mu_{\mathcal{L}}, \mu_{\mathcal{R}} > 0$ there exists an infinite number of border collision bifurcation curves separating regions of existence of periodic orbits with arbitrarily high periods. These are organized by the so-called *period adding* phenomenon. To explain this, we first introduce the usual symbolic dynamics.

Let us assume that $(x_1, \ldots, x_n)$ is an n-periodic orbit of the map (2.7). To this periodic orbit we assign a symbolic encoding given by

$$(2.8) \qquad \begin{aligned} x_i &\to \mathcal{L} \quad \text{if } x_i < 0, \\ x_i &\to \mathcal{R} \quad \text{if } x_i > 0. \end{aligned}$$

For each periodic orbit we obtain a symbolic sequence of $\mathcal{L}$'s and $\mathcal{R}$'s depending on whether the orbit steps on the left or on the right of the boundary. Obviously, the length of the symbolic sequence is the period of the periodic orbit.

Then, the period adding structure is described as follows. Between the regions of existence of periodic orbits with symbolic sequences σ_1 and σ_2 and periods n_{σ_1} and n_{σ_2} there exists a region corresponding to the existence of a periodic orbit with symbolic sequence $\sigma_1 \sigma_2$. Clearly, the period of this periodic orbit is $n_{\sigma_1} + n_{\sigma_1}$. This occurs ad infinitum, as illustrated in Figure 2(b), where one can see the periods of the periodic orbits obtained when crossing all these regions along a curve such as that shown in Figure 2(a).

Beyond the evolution of the periods of the periodic orbits, one of the most relevant quan-
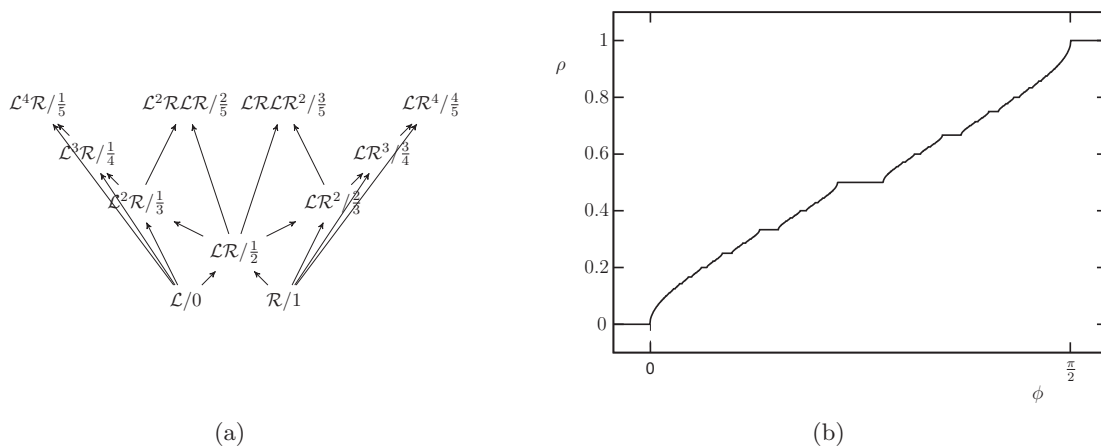
Figure 3. (a) *Symbolic sequences and rotation numbers forming a Farey tree structure for the period adding bifurcation.* (b) *Devil's staircase associated with the rotation numbers along the Farey tree, obtained along a curve such as the one labeled in Figure* 2(a).

tities associated with the adding scheme is the *rotation number* corresponding to the periodic orbits obtained when crossing all these regions in the parameter space. As shown in Figure 3(a), the rotation number associated to each periodic orbit is obtained by dividing the number of $\mathcal{R}$ symbols contained in its symbolic sequence by the period of the periodic orbit (see [GGT84, GIT84]). Hence, the rotation number follows a *devil's staircase* from 0 to 1 when parameters are varied along curves such as that shown in Figure 2(a). A devil's staircase is a monotonically increasing continuous function which is constant almost everywhere, except for a Cantor set of zero measure. In this Cantor set, which consists of the border collision bifurcation curves shown in Figure 2(a), the rotation number becomes irrational and no periodic orbit exists, but there exists a quasi-periodic orbit.

The period adding phenomenon described above was first described in [GGT84] and was later studied in more detail in [GPTT86, LPZ89, TS86, PTT87, Gam87, GT88]. Subsequently, this was rediscovered when the authors of [AS06] were numerically investigating map (2.7) with $g_{\mathcal{L}}$ and $g_{\mathcal{R}}$ linear functions. The authors of [AS06] provided an accurate description of the bifurcation scenario in terms of nonsmooth language (border collision bifurcations). Special attention was given to the codimension-two bifurcation at the origin of the $(\mu_{\mathcal{L}}, \mu_{\mathcal{R}})$-parameter space, which was called the *period adding big bang* bifurcation, to distinguish it from the so-called *period incrementing big bang* bifurcation, both being a special type of the *gluing* bifurcation reported in [CGT84, GGT88]. The period incrementing case, which exhibits a completely different bifurcation scenario, occurs when one of the functions $g_{\mathcal{L}}$ or $g_{\mathcal{R}}$ is decreasing and the other one is increasing near the origin (both being contracting functions), as was rigorously proven in [AGS11]. As mentioned above, a proof for the period adding bifurcation structure can be found in the recent review article [GAK14].

Theorem 2.1. *Let g be a map as in* (2.7) *such that* $g_{\mathcal{L}}$ *and* $g_{\mathcal{R}}$ *are increasing contracting*

functions:

$$0 < (g_{\mathcal{L}}(x))' < 1, \quad x \in (-\infty, 0),$$
$$\text{(2.9)} \qquad 0 < (g_{\mathcal{R}}(x))' < 1, \quad x \in (0, \infty).$$

Consider a C^1 curve in the $(\mu_{\mathcal{L}}, \mu_R)$-parameter space

$$\gamma : \begin{array}{ccc} [0,1] & \longrightarrow & \mathbb{R}^2 \\ \lambda & \longmapsto & (\mu_{\mathcal{L}}(\lambda), \mu_{\mathcal{R}}(\lambda)) \end{array},$$

satisfying

    C.1. *$\mu_{\mathcal{L}}(\lambda) > 0$ and $\mu_{\mathcal{R}}(\lambda) > 0$ for $\lambda \in (0,1)$;*
    C.2. *$(\mu_{\mathcal{L}}(\lambda))' > 0$ and $(\mu_{\mathcal{R}}(\lambda))' < 0$ for $\lambda \in [0,1]$; and*
    C.3. *$\mu_{\mathcal{L}}(0) = 0$, $\mu_{\mathcal{R}}(1) = 0$.*

Then, the bifurcation diagram exhibited by the map g_λ obtained from (2.7) after performing the reparametrization given by γ follows a period adding structure for $\lambda \in [0,1]$. Moreover, the rotation number $\rho(g_\lambda)$ of the map g_λ is a devil's staircase as a function of λ such that $\rho(g_0) = 0$ and $\rho(g_1) = 1$.

    Remark 2.1. The increasing and contractive condition (2.9) can be relaxed to be satisfied locally near $x = 0$ if $\mu_{\mathcal{L}}(\lambda)$ and $\mu_{\mathcal{R}}(\lambda)$ are small enough for $\lambda \in (0,1)$. This is because the periodic orbits are located in the absorbing interval $[-\mu_{\mathcal{R}}(\lambda), \mu_{\mathcal{L}}(\lambda)]$.

    By means of Theorem 2.1 we will show that the stroboscopic map follows period adding bifurcation structures when the parameters A and d are varied along curves as the straight line shown in Figure 1(a): the white regions in Figure 1 surrounded by gray regions are filled by the bifurcation structures shown in Figure 2. We will use the properties of the devil's staircase of the rotation number to deduce properties of the firing rate defined in (2.6).

3. Dynamics of the stroboscopic map.

3.1. Notation, properties, and subthreshold dynamics. Let

$$\text{(3.1)} \qquad \varphi(t; x_0; A)$$

be the flow associated with system

$$\text{(3.2)} \qquad \dot{x} = f(x) + A$$

such that $\varphi(0; x_0; A) = x_0$. As usual in piecewise-defined systems, by properly concatenating the flows $\varphi(t; x_0; A)$, $\varphi(t; x_0; 0)$ and the reset condition (2.3) one obtains the flow

$$\text{(3.3)} \qquad \phi(t; x_0)$$

associated with system (2.1)–(2.3) such that $\phi(0; x_0) = x_0$. Due to the reset conditions, this flow is discontinuous at the times for which spikes occur. In addition, due to the discontinuities of the forcing $I(t)$ defined in (2.2), the flow ϕ is nondifferentiable at $t = dT \mod T$.

    Note that for the definition of the flow ϕ associated with the nonautonomous system (2.1) we consider that the initial condition x_0 occurs at $t_0 = 0$. This will be assumed in the rest of

this work and, as we are interested in the existence of periodic orbits, does not present any loss of generality.

Under assumptions H.1–H.2 we first study the subthreshold dynamics, that is, invariant objects of system (2.1)–(2.3) that do not interact with the threshold (do not exhibit spikes).

On one hand, if $d = 0$, then $I(t) = 0$, and system (2.1)–(2.3) has the same dynamics as the autonomous system (2.4). That is, it has an attracting equilibrium point at $x = \bar{x}$.

On the other hand, if $d = 1$, then $I(t) = A$. Hence system (2.1)–(2.3) becomes the autonomous system (3.2) subject to the reset condition (2.3), and, as for $d = 0$, the T-periodic forcing does not play any role. By the implicit function theorem, if $A > 0$ is small enough, the system possesses an attracting equilibrium point at

$$x^* = \bar{x} - \frac{A}{f'(\bar{x})} + O(A^2) < \theta.$$

Note that, as $f(x)$ is a monotonically decreasing function (condition H.2), this equilibrium point increases with A toward the boundary $x = \theta$. Thus, for $d = 1$, when A is large enough, this equilibrium point collides with the boundary $x = \theta$ and undergoes a border collision bifurcation. After this bifurcation, the system has a periodic orbit that spikes once per period. The period of this periodic orbit, $\delta > 0$, becomes the time needed by system $\dot{x} = f(x) + A$ with initial condition $x_0 = 0$ to reach the threshold $x = \theta$. This is the smallest $\delta > 0$ such that

$$(3.4) \qquad\qquad\qquad\qquad \varphi(\delta; 0; A) = \theta,$$

if it exists (A is large enough).

Let us now study the subthreshold dynamics of the system when $0 < d < 1$. We have the following proposition.

Proposition 3.1. *Let*

$$Q := \frac{1}{T} \int_0^T I(t)dt = Ad$$

be small enough. Then, if $T > 0$ is small enough, system (2.1)–(2.3) has a T-periodic orbit that does not hit the boundary $x = \theta$.

Proof. The proof is accomplished by averaging the system. After the time rescaling $\tau = \frac{t}{T}$ system (2.1) becomes

$$(3.5) \qquad\qquad\qquad\qquad \dot{x} = T\left(f(x) + I(\tau T)\right),$$

where $\dot{}$ now means the derivative with respect to τ and $I(\tau T)$ is 1-periodic. We now consider the averaged version of system (3.5),

$$(3.6) \qquad\qquad\qquad\qquad \dot{y} = T\left(f(x) + Q\right).$$

By the averaging theorem, as system (3.5) is Lipschitz in x, if system (3.6) possesses a hyperbolic equilibrium point, then, for $T > 0$ small enough, system (3.5) possesses a hyperbolic

periodic orbit (see [BM61, GH83]). This will occur if $Q > 0$ is small enough, and the equilibrium point of (3.6) will be of the form

$$\bar{y} = \bar{x} - \frac{Q}{f'(\bar{x})} + O\left(Q^2\right) < \theta,$$

where $\bar{x}$ is the hyperbolic equilibrium point of system (2.4).

Then, the periodic orbit of system (3.5) will be T-close to $\bar{y}$. ∎

When A is large, the periodic orbit given by the previous lemma may undergo a border collision bifurcation and lead to spiking dynamics. This new dynamics will be studied in sections 3.2 and 3.3 by means of the stroboscopic map, i.e., the time-T return map

$$(3.7) \qquad \begin{array}{rccc} \mathfrak{s}: & [0, \theta) & \longrightarrow & [0, \theta) \\ & x_0 & \longmapsto & \phi(T; x_0) \end{array}.$$

The main results in this work rely on the fact that $\mathfrak{s}$ is a piecewise-smooth map. To see this, we define the sets

$$(3.8) \qquad \begin{aligned} S_n = \Big\{ x_0 \in [0, \theta) \text{ s.t. } \phi(t; x_0) \text{ reaches the threshold } \{x = \theta\} \\ n \text{ times for } 0 \leq t \leq T \Big\}, \quad n \geq 0. \end{aligned}$$

When restricted to some set S_n, the flow $\phi(t; x_0)$ becomes a certain combination of the smooth flows $\varphi(t; x_0; A)$, $\varphi(t; x_0; 0)$ and the smooth mapping $\theta \mapsto 0$ (given by the reset condition) which does not depend on the initial condition $x_0 \in S_n$. Hence, the stroboscopic map $\mathfrak{s}$ becomes a smooth map in each of the sets S_n and is as regular as the flow $\varphi(t; A)$. Given $m \neq n$, the flow, when restricted to S_n and S_m, performs a different number of spikes in the time window $[0, T]$. Hence $\mathfrak{s}$ is given by a different combination of the mentioned maps. Thus, $\mathfrak{s}$ is smooth on the interiors of S_n and S_m but will typically be discontinuous at its boundaries. As will be discussed below (see Remark 3.2), the stroboscopic map remains discontinuous even if one identifies $0 \sim \theta$ and considers system (2.1)–(2.3) in the circle.

Note that some of the sets S_n may be empty. The next lemma tells us that at most two of them are nonempty and that they must be consecutive (see Figure 4 for S_2 and S_3). Moreover, let $\Sigma_n \in S_n$ be defined by the requirement

$$(3.9) \qquad \phi(dT; \Sigma_n) = \theta.$$

That is, Σ_n is the (unique) initial condition whose trajectory spikes n times and performs its last spike precisely at $t = dT$. The next lemma tells us also that Σ_n is the value at which the map $\mathfrak{s}$ exhibits a discontinuity and separates the sets S_{n-1} and S_n.

Lemma 3.1. *Assume that there exists $\Sigma_n \in S_n$ as given in (3.9) for some $n \geq 1$. Then the following statements hold:*
  (i) *If $\Sigma_i, \Sigma_j \in [0, \theta)$, then $i = j$.*
  (ii) *If $\Sigma_n \in (0, \theta)$, then $[0, \Sigma_n) = S_{n-1}$ and $[\Sigma_n, \theta) = S_n$.*
  (iii) *If $\Sigma_n = 0$, then $[0, \theta) = S_n$.*
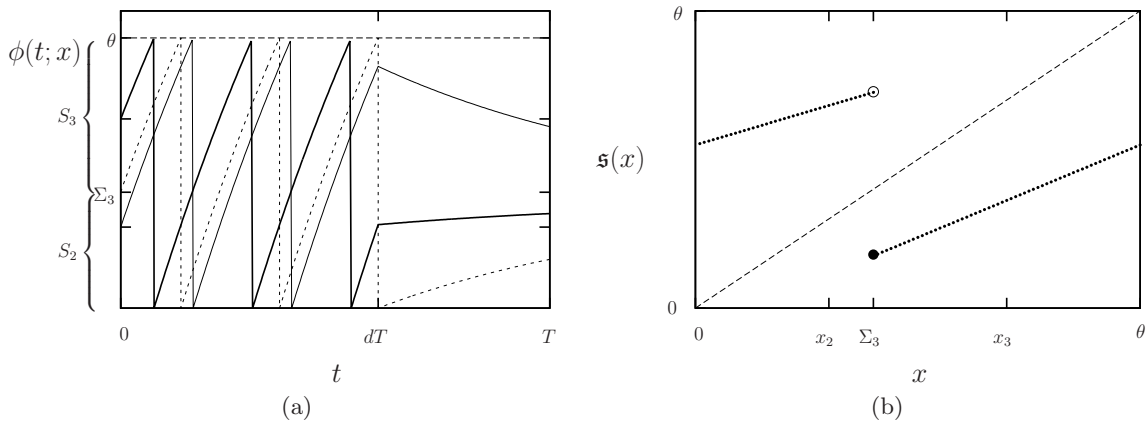
Figure 4. (a) *The trajectories of systems* (2.1)–(2.3). *Dashed line: Trajectory with Σ_3 as initial condition. Thick line: Trajectory with $x_3 > \Sigma_3$ as initial condition, which spikes three times. Normal line: Trajectory with $x_2 < \Sigma_3$ as initial condition, which spikes two times.* (b) *The stroboscopic map, with a discontinuity at $x = \Sigma_3$.*

Proof. Part (i) comes from the fact that the flow ϕ is invertible. Hence, if it exists, the initial condition that makes ϕ reach θ at $t = dT$ is unique.

We now prove (ii). Let

$$(3.10) \qquad t_n < t_n + \delta < \cdots < t_n + (n-2)\delta < t_n + (n-1)\delta = dT$$

be the sequence of times for which the trajectory $\phi(t; \Sigma_n)$ exhibits spikes. Let us now take an initial condition $x_0 < \Sigma_n$. For $t < dT$ the flow $\phi(t; x_0)$ becomes the flow of the autonomous system $\dot{x} = f(x) + A$ plus the reset condition (2.3). Hence, the first spike of the trajectory $\phi(t; x_0)$ occurs for $t > t_n$. By induction, the $n-1$th spike for such a trajectory occurs for $t \in (dT - \delta, dT)$, with δ as in (3.4). For $t > dT$ the trajectory $\phi(t; x_0)$ becomes the flow of system $\dot{x} = f(x)$, which has an attractor $\bar{x} \in (0, \theta)$; hence, no other spikes can occur for $t > dT$, and the trajectory $\phi(t; x_0)$ exhibits exactly $n-1$ spikes for $0 \le t \le T$. Using (i), we get that $[0, \Sigma_n) = S_{n-1}$. Arguing similarly, any trajectory $\phi(t; x_0)$ with $x_0 \in [\Sigma_n, \theta)$ exhibits exactly n spikes for $0 \le t \le T$, and thus $[\Sigma_n, \theta) = S_n$.

Proceeding similarly, if $\Sigma_n = 0$, then all initial conditions in $[0, \theta)$ lead to trajectories exhibiting an nth spike for $t \in (dT - \delta, dT)$. Hence, $S_n = [0, \theta)$. ∎

Remark 3.1. The values Σ_n become upper and lower boundaries of the sets S_{n-1} and S_n, respectively.

The following results give us properties of the boundaries Σ_n which we will use in section 3.2.

Lemma 3.2. *Let $d \in (0,1)$ and $A > 0$, and assume $\Sigma_n \in (0, \theta)$. Then Σ_n is a monotonically decreasing function of A.*

Proof. To avoid confusion with the differential and derivative, in this proof we rename the duty cycle d as a.

The boundary Σ_n is determined by the initial condition such that the flow $\phi(t; x_0)$ collides with the boundary for the nth time at $t = aT$. Let $\varphi(t; x_0; A)$ be the flow defined in (3.1),

and let $\delta > 0$ be as in (3.4) and (3.10), i.e., the time needed for the trajectory with initial condition $x_0 = 0$ to reach the threshold θ, as defined in (3.4). Note that δ is a decreasing function of A. In fact, rewriting (3.4) as

$$\int_0^\theta \frac{dx}{f(x) + A} = \delta,$$

we get that

$$\frac{d\delta}{dA} = -\int_0^\theta \frac{dx}{(f(x) + A)^2} < 0.$$

The boundary Σ_n is thus determined by the equation

$$\varphi(aT - (n-1)\delta; \Sigma_n, A) = \theta,$$

or, equivalently, by the equation

$$\int_{\Sigma_n}^\theta \frac{dx}{f(x) + A} = aT - (n-1)\delta.$$

Differentiating, we get that

$$\frac{d\Sigma_n}{dA} = -(f(\Sigma_n) + A)\left(\int_{\Sigma_n}^\theta \frac{dx}{(f(x) + A)^2} - (n-1)\frac{d\delta}{dA}\right).$$

Noting that $f(\Sigma_n) + A > 0$ because the system $\dot{x} = f(x) + A$ possesses an attracting equilibrium point for $x > \theta$ (which permits it to spike), we get that

$$\frac{d\Sigma_n}{dA} < 0. \qquad \blacksquare$$

The next lemma provides the lateral values of the stroboscopic map $\mathfrak{s}$ at the discontinuities.

Lemma 3.3. *Let*

(3.11) $\mathfrak{s}_- = \varphi(T(1-d); \theta; 0),$

(3.12) $\mathfrak{s}_+ = \varphi(T(1-d); 0; 0),$

where $\varphi(t; x_0; A)$ is the flow defined in (3.1).
    If $\Sigma_n \in [0, \theta)$, then the lateral images of Σ_n by $\mathfrak{s}$ do not depend on A or n and become

(3.13) $\mathfrak{s}(\Sigma_n^-) = \mathfrak{s}_-,$

(3.14) $\mathfrak{s}(\Sigma_n^+) = \mathfrak{s}_+.$

Proof. The trajectory of Σ_n is such that the flow $\phi(t; \Sigma_n)$ reaches the threshold for the nth time exactly at $t = dT$. The limiting value $\mathfrak{s}(\Sigma_n^-)$ is obtained assuming that the flow does not spike at $t = dT$ (the threshold is almost reached). Hence, one just needs to integrate the flow $\varphi(t; x_0; 0)$ from $t = dT$ to $t = T$ with initial condition $x_0 = \theta$. This gives (3.13).

On the other hand, the right image is computed by adding a new spike at $t = dT$. Hence, one has only to proceed identically but replacing the initial condition by that given by the reset, $x_0 = 0$. ∎

Remark 3.2. Due to the fact that $f(0) \neq f(\theta)$, if one identifies $0 \sim \theta$, the field (2.1) becomes discontinuous. For the initial condition $x = \Sigma_n$ the flow grazes, that is, it has contact points with the threshold without crossing it. Hence, even when considering system (2.1)–(2.3) in the circle, the stroboscopic map is still discontinuous at $x = \Sigma_n$.

Lemma 3.4. *The following facts hold:*

(i) *For any $n \geq 1$, the stroboscopic map restricted to $[0, \Sigma_n)$ is always contracting.*

(ii) *If n is large enough, $\mathfrak{s}$ is also contracting in $[\Sigma_n, \theta)$.*

Proof. Let δ be as defined in (3.4) and $x \in [0, \Sigma_n)$. Note that $\phi(i\delta; x) = x$ for all x and $0 \leq i \leq n$, where $\phi(t; x)$ is the flow with the resets defined in (3.3). Let $\varepsilon = dT - (n-1)\delta$. Then, when restricted to $[0, \Sigma_n)$, the stroboscopic map becomes

$$\mathfrak{s}(x) = \varphi(T - dT; \varphi(\varepsilon; x; A); 0).$$

The fact that ε does not depend on x guarantees that $\mathfrak{s}(x)$ is contracting, as it becomes the (continuous) concatenation of two contracting flows using x as initial condition. This proves (i).

In order to prove (ii), let $x \in [\Sigma_n, \theta)$ and $\varepsilon = n\delta - dT$. Then, $\mathfrak{s}(x)$ becomes

$$\mathfrak{s}(x) = \varphi(T - dT; \varphi^{-1}(\varepsilon; x; 0); A).$$

We now compute $\mathfrak{s}'(x)$:

$$(3.15) \qquad \mathfrak{s}'(x) = \exp\left(-\int_{dT}^{n\delta} f'(\varphi(t; x; A))dt + \int_{dT}^{T} f'(\varphi(t; x; 0))dt\right).$$

Recall that f' is a negative function, and note that δ is a function of A satisfying $n\delta - dT < \delta$ and $(n-1)\delta < dT$. Hence, for M satisfying $|f'(x)| \leq M$ for all $x \in [0, \theta]$, we get

$$-\int_{dT}^{n\delta} f'(\varphi(t; x; A))dt \leq \delta M \leq M\frac{dT}{n-1}.$$

Hence, for n large enough, $\mathfrak{s}'(x) < 1$ for all $x \in [\Sigma_n, \theta)$. ∎

3.2. Border collision bifurcations of spiking fixed points. As noted in the previous section, nonspiking periodic orbits (without interaction with the threshold) exist for $A > 0$ small enough and $d = 0$ or $d = 1$. Hence, the natural parameter space in which to study the possible bifurcations leading to spiking dynamics is (d, A). Equivalently, we will consider $(d, 1/A)$ instead. This is because, in this space, the bifurcation curves will be bounded.

In order to show that the bifurcation scenario in the $(d, 1/A)$-parameter space for system (2.1)–(2.3) is equivalent to that shown in Figure 1 and described in section 2, we first show the existence of an infinite number of regions for which $\mathfrak{s}$ possesses fixed points. These fixed points are located at different domains S_n defined in (3.8). These regions in the parameter space are the gray regions in Figure 1. As shown in the next result, when they exist,

these fixed points are unique and are located at one side of some discontinuity Σ_n. By varying parameter values, they bifurcate when entering the white regions in Figure 1(a).

The next proposition provides the existence of unique fixed points, $\bar{x}_n \in S_n$ for any $n \geq 0$.

Proposition 3.2. Let $d \in (0,1)$ and $n \geq 0$. Then, there exists some value of A for which the stroboscopic map $\mathfrak{s}$ defined in (3.7) possesses an attracting fixed point $\bar{x}_n \in S_n$. When it exists, this fixed point becomes the only invariant object of $\mathfrak{s}$.

Proof. The existence of the fixed point $\bar{x}_0 \in S_0$ of the stroboscopic map $\mathfrak{s}$ (3.7) for any $d \in (0,1)$ when $A > 0$ is small enough comes from Proposition 3.1. By induction we now show that, for any $n \geq 0$, there exist values of A for which one finds fixed points $\bar{x}_n$ of $\mathfrak{s}$ leading to periodic orbits spiking n times: $\bar{x}_n \in S_n$. Assume that there exists a fixed point $\bar{x}_{n-1} \in S_{n-1}$. By increasing A if necessary, we can assume that $S_{n-1} = [0, \Sigma_n)$ ($\bar{x}_{n-1}$ is located at the left of the discontinuity). Then, by Lemma 3.2, Σ_n is a monotonically decreasing function of A. Hence, by further increasing A, one necessarily finds some value $A = A_n^{\mathcal{C}}(d)$ for which $\Sigma_n = 0$. At this point, by Lemma 3.1(iii), we get that $[0, \theta) = S_n$, and the map $\mathfrak{s}$ becomes continuous and contracting (see Lemma 3.4). Hence, as $\mathfrak{s}(S_n) \subset S_n$, there necessarily exists a fixed point $\bar{x}_n \in S_n$ for $A = A_n^{\mathcal{C}}(d)$ which is attracting and the unique invariant object.

We now show that, in general, when they exist, the fixed points $\bar{x}_n$ are attracting and the only possible invariant objects. On one hand, note that the stroboscopic map is monotonically increasing. On the other hand, we recall that, from Lemma 3.1, we use that at most two sets S_{n-1} and S_n or S_n and S_{n+1} can coexist. Hence, if $\mathfrak{s}$ possesses a fixed point $\bar{x}_n \in S_n$, there exist only three possible situations:

1. $\bar{x}_n \in (0, \theta) \subset S_n$;
2. $[0, \Sigma_n) = S_{n-1}$ and $\bar{x}_n \in [\Sigma_n, \theta) = S_n$; and
3. $\bar{x}_n \in (0, \Sigma_{n+1}) \subset S_n$ and $[\Sigma_{n+1}, \theta) = S_{n+1}$.

Note that $\bar{x} \in (0, \theta)$ implies that necessarily $\bar{x}_n \neq 0$.

The first case leads to the situation considered above, as the map is continuous ($\Sigma_n = 0$).

In the second and third cases we argue below as before and also using the fact that $\mathfrak{s}$ has a negative gap at its discontinuities (illustrated in Figure 6); that is,

$$\lim_{x \to (\Sigma_n)^-} \mathfrak{s}(x) > \lim_{x \to (\Sigma_n)^+} \mathfrak{s}(x) \quad \forall n \geq 0$$

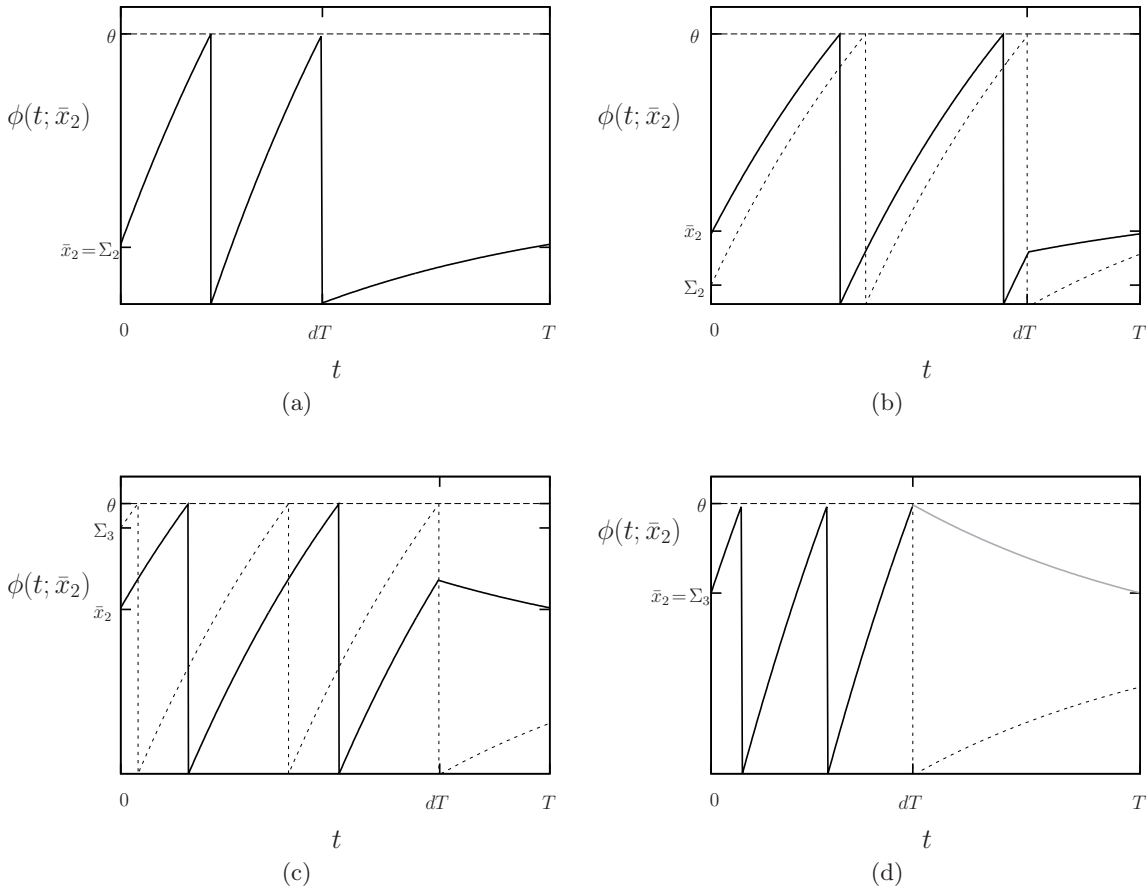(see Figure 4 for $n = 3$). This is a direct consequence of Lemma 3.3.

In the third case, contractiveness comes from Lemma 3.4(i). In the second case, we rewrite expression (3.15) integrating with respect to x instead of t, and we get

$$\mathfrak{s}'(\bar{x}_n) = \exp\left(-\int_y^{\bar{x}_n} \frac{f'(x)}{f(x) + A} dx + \int_y^{\bar{x}_n} \frac{f'(x)}{f(x)} dx\right),$$

where $y = \varphi^{-1}(n\delta - dT; \bar{x}_n; A)$. As $\bar{x}_n < \bar{x}$,

$$-\frac{f'(x)}{f(x) + A} < \frac{f'(x)}{f(x)} < 0.$$

Hence $\mathfrak{s}'(\bar{x}_n) < 1$, as both functions are integrated along the same interval. ∎

Figure 5. *T-periodic orbit spiking twice per period (fixed point $\bar{x}_2$ of the stroboscopic map) and its bifurcations when A is varied along $(A_2^{\mathcal{R}}(d), A_2^{\mathcal{L}}(d))$. It undergoes border collision bifurcations when it collides with the boundaries Σ_2 and Σ_3, (a) and (d), respectively. The periodic orbit shown in (d) is its limit when $\bar{x}_2 \to \Sigma_3^-$; note that for $\bar{x}_2 = \Sigma_3$ it should be reset to 0 at $t = dT$; this is why it is shown in gray. In (b) and (c), the trajectories of these boundaries are shown in dashed lines; note that they collide with the threshold at $t = dT$. Parameter values for panel (c) are the same as for point D of Figure 1(a). The four figures are in one-to-one correspondence with the four figures of Figure 6, where the stroboscopic map is shown.*

The next proposition provides us with the bifurcation curves at which the fixed points $\bar{x}_n \in S_n$ given in Proposition 3.2 undergo border collision bifurcations, that is, curves for which the fixed points collide with the boundaries:

$$A \longrightarrow A_n^{\mathcal{L}}(d) \Longrightarrow \bar{x}_n \longrightarrow (\Sigma_n)^-, \quad n \geq 0,$$
$$A \longrightarrow A_n^{\mathcal{R}}(d) \Longrightarrow \bar{x}_n \longrightarrow (\Sigma_{n-1})^+, \quad n \geq 1.$$

Note that $\bar{x}_0$ can undergo only one bifurcation—for $A = A_0^{\mathcal{L}}(d) := A_0(d)$.

Proposition 3.3. *For any $0 < d < 1$ there exists a sequence*

$$(3.16) \qquad 0 < A_0(d) < A_1^{\mathcal{R}}(d) < A_1^{\mathcal{L}}(d) < A_2^{\mathcal{R}}(d) < A_2^{\mathcal{L}}(d) < \dots,$$
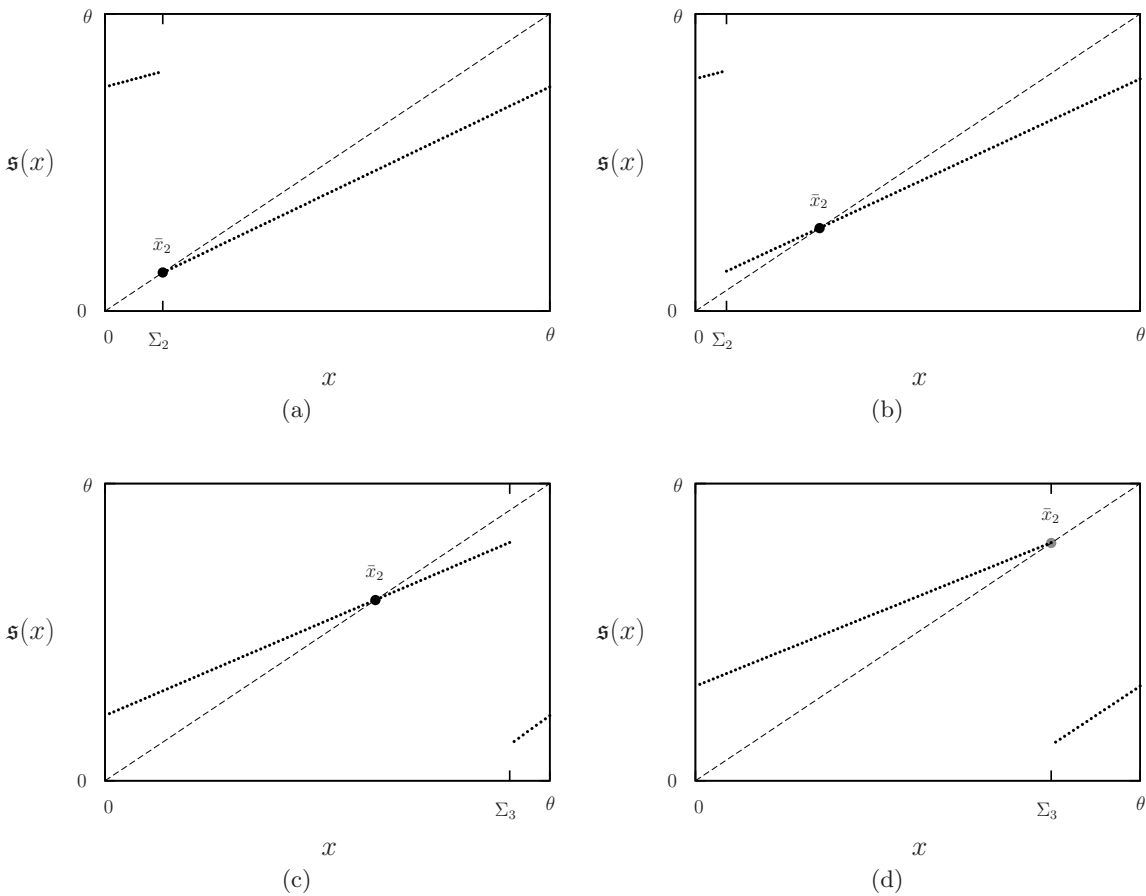
Figure 6. *Stroboscopic map for the T-periodic orbits shown in Figure 5. In (a) and (d) the fixed point $\bar{x}_2$ undergoes a border collision bifurcation when it collides with the boundaries Σ_2 from the right and Σ_3 from the left, respectively. Note that, in (d) the fixed point is shown in gray to emphasize that the map indeed takes the value on the right for $x = \Sigma_3$. In (b)–(c) the boundary Σ_2 disappears, and a new boundary Σ_3 appears, while the fixed point $\bar{x}_2$ remains.*

such that, for every $n > 0$, the stroboscopic map $\mathfrak{s}$ (3.7) possesses a unique fixed point $\bar{x}_n \in S_n$ for $A \in (A_n^{\mathcal{R}}(d), A_n^{\mathcal{L}}(d))$. This fixed point undergoes a border collision bifurcation at $A = A_n^{\mathcal{L}}(d)$ and $A = A_n^{\mathcal{R}}(d)$.

The values $A_0(d)$, $A_n^{\mathcal{L}}(d)$, and $A_n^{\mathcal{R}}(d)$ define smooth curves fulfilling

$$\lim_{d \to 0} A_0 = \infty,$$
$$\lim_{d \to 0} A_n^{\mathcal{R}, \mathcal{L}}(d) = \infty.$$

Hence these curves go through the origin of the $(d, 1/A)$-parameter space. Moreover,

$$(3.17) \qquad\qquad \lim_{d \to 1} A_n^{\mathcal{R}}(d) = \lim_{d \to 1} A_n^{\mathcal{L}}(d), \quad n \geq 1,$$

and this limit becomes the value of A for which

$$\delta = \frac{T}{n},$$

where δ is as defined in (3.4).

Proof. Let $\mathfrak{s}_-$ and $\mathfrak{s}_+$ be as in (3.11) and (3.12):

$$\mathfrak{s}_- = \varphi(T(1-d); \theta; 0),$$
$$\mathfrak{s}_+ = \varphi(T(1-d); 0; 0).$$

As given in Lemma 3.3, if the stroboscopic map exhibits a discontinuity, $\Sigma_n \in (0, \theta)$, then these values coincide with the lateral images of Σ_n:

$$\mathfrak{s}(\Sigma_n^-) = \mathfrak{s}_-,$$
$$\mathfrak{s}(\Sigma_n^+) = \mathfrak{s}_+.$$

For $0 < d < 1$ and $n \geq 1$, let $A_n^{\mathcal{C}}(d)$ be as in the proof of Proposition 3.2, i.e., the value of A defined by the condition $\Sigma_n = 0$. By Lemma 3.2 and the implicit function theorem, $A_n^{\mathcal{C}}(d)$ is a smooth function of d. We begin by discussing the bifurcation sequence occurring for some $0 < d < 1$ and $0 < A < A_1^{\mathcal{C}}(d)$. The sequence of bifurcations that we now describe is illustrated in Figure 9 for a particular example.

First note that for A sufficiently small, $[0, \theta) = S_0 \cup S_1$ and $\Sigma_1 > \mathfrak{s}_- = \mathfrak{s}(\Sigma_1^-)$. In this case the graph of $\mathfrak{s}$ is as shown in Figure 6(c) (for $n = 3$), and clearly the fixed point $\bar{x}_0$ contained in S_0 must exist (see Figure 5(c)). By Lemma 3.2, when A is increased, Σ_1 decreases with nonzero speed. Hence there exists a unique value of $A = A_0$ such that $\Sigma_1 = \mathfrak{s}_- = \mathfrak{s}(\Sigma_1^-)$ (see Figure 6(d) for Σ_3). In other words, the fixed point $\bar{x}_0$ undergoes a border collision bifurcation as it collides with the boundary Σ_1 on its left (see Figure 5(d)). Moreover, by Lemma 3.2 and the implicit function theorem, the equation $\Sigma_1 = \mathfrak{s}_-$ defines a smooth function $A_0(d)$.

For $A > A_0(d)$ the map $\mathfrak{s}$ is as shown in Figure 4(b), and the fixed point $\bar{x}_0$ no longer exists. As A is further increased, Σ_1 crosses $\mathfrak{s}_+$ for some value $A = A_1^{\mathcal{R}}$. For this value, the fixed point $\bar{x}_1$ undergoes a border collision bifurcation as it collides with the boundary Σ_1 on its right (see Figures 5(a) and 6(a) for $\bar{x}_2$). Similarly as above, the equation $\Sigma_1 = \mathfrak{s}_+$ defines a smooth function $A = A_1^{\mathcal{R}}(d)$, and for $A > A_1^{\mathcal{R}}(d)$ the fixed point $\bar{x}_1$ exists. Finally, for $A = A_1^{\mathcal{C}}(d)$ the map is continuous on the entire $(0, \theta)$ with fixed point $\bar{x}_1$.

We now repeat the same argument to show that the same bifurcation sequence occurs for $A_n^{\mathcal{C}}(d) < A \leq A_{n+1}^{\mathcal{C}}(d)$, $n \geq 1$. Indeed, for $A > A_n^{\mathcal{C}}(d)$ but close to $A_n^{\mathcal{C}}(d)$, we have $\Sigma_n > \mathfrak{s}_-$. In this case the graph of $\mathfrak{s}$ is again as shown in Figure 6(c), and clearly the fixed point $\bar{x}_{n-1}$ contained in S_{n-1} must exist (see Figure 5(c)). By Lemma 3.2, when A is increased, Σ_n decreases with nonzero speed. Hence there exists a unique value of $A = A_{n-1}^{\mathcal{L}}$ such that $\Sigma_n = \mathfrak{s}_- = \tilde{\mathfrak{s}}(\Sigma_n^-)$ (see Figures 5(d) and 6(d) for $n = 3$). For this value of A, the fixed point $\bar{x}_{n-1}$ undergoes a border collision as it collides with the boundary Σ_n on its left. Moreover, by Lemma 3.2 and the implicit function theorem, the equation $\Sigma_n = \mathfrak{s}_- = \mathfrak{s}(\Sigma_n^-)$ defines a smooth function $A_n^{\mathcal{L}}(d)$.

For $A > A_{n-1}^{\mathcal{L}}(d)$ the map $\mathfrak{s}$ is as shown in Figure 4(b), and the fixed point $\bar{x}_{n-1}$ no longer exists. As A is further increased, there exists some value $A = A_n^{\mathcal{R}}(d)$ for which Σ_n crosses $\mathfrak{s}_+$,

as in Figure 6(a). For this value, the fixed point $\bar{x}_n$ undergoes a border collision bifurcation as it collides with the boundary Σ_n on its right (see Figure 5(a) for $n = 3$). Similarly as above, the equation $\Sigma_n = \mathfrak{s}_+ = \mathfrak{s}(\Sigma_n^+)$ defines a smooth function $A = A_n^{\mathcal{R}}(d)$, and for $A > A_n^{\mathcal{R}}(d)$ the fixed point $\bar{x}_n$ exists. Finally, for $A = A_n^{\mathcal{C}}(d)$ the map is continuous on the entire $(0, \theta)$ with fixed point $\bar{x}_n$.

Finally, note that due to the fact that the lateral values of Σ_n by $\mathfrak{s}$ ($\mathfrak{s}_-$ and $\mathfrak{s}_+$) do not depend on A and, by Lemma 3.2, Σ_n monotonically decreases with A, the bifurcations described above, given by $\mathfrak{s}(\Sigma_n^\pm) = \mathfrak{s}_\pm$, can occur only once if A is monotonically varied.

As will be shown in next section, the periodic orbits that exist in the intervals of the form $(A_{n-1}^{\mathcal{L}}(d), A_n^{\mathcal{R}}(d))$ are given by the period adding structure.

We now discuss the limiting values of the curves $A_n^{\mathcal{R},\mathcal{L}}(d)$ when $d \to 0$ and $d \to 1$.

Let $A_0(d)$ be the curve where the fixed point $\bar{x}_0 \in S_0$ undergoes a border collision. As discussed above, this occurs when the fixed point $\bar{x}_0$ collides with the boundary:

$$(3.18) \qquad \varphi(dT; \bar{x}_0; A_0) = \theta,$$
$$\varphi(T - dT; \theta; 0) = \bar{x}_0,$$

where $\varphi(t; x; A)$ is the flow associated with system $\dot{x} = f(x) + A$. As the field $f(x) + A$ increases with A, $\varphi(dT; x; A)$ is a monotonically increasing function of A for $A \in [A_0, A_1^{\mathcal{R}})$ for all $x \in [0, \theta)$. Hence, if $d \to 0$, then $A_0 \to \infty$ in order to keep (3.18) satisfied. Therefore, the curve defined by $A_0(d)$ goes through the origin of the $(d, 1/A)$-parameter space. The sequence given in (3.16) implies that all the other bifurcation curves given by $A_n^{\mathcal{R},\mathcal{L}}(d)$ also go through this point.

We now focus on $d \to 1$. Let $A \in (A_n^{\mathcal{R}}(d), A_n^{\mathcal{L}}(d))$, and hence there exists a fixed point $\bar{x}_n \in S_n$ of $\mathfrak{s}$. In order to see (3.17) we will show that, if there exists such a fixed point, then necessarily $\mathfrak{s}(x) \to x$ when $d \to 1$; that is, if a fixed point exists, then the stroboscopic map $\mathfrak{s}$ tends to the identity when $d \to 1$. If that is the case, then both bifurcations tend to occur at the same time, and hence

$$A_n^{\mathcal{R}}(d) - A_n^{\mathcal{L}}(d) \to 0,$$

and both limits exist, which proves (3.17).

To see that $\mathfrak{s}$ tends to the identity when $d \to 1$ if $\bar{x}_n \in S_n$, we first recall that for $d = 1$ system (2.1)–(2.3) becomes the autonomous system $\dot{x} = f(x) + A$ plus the reset condition (2.3). As $A \in (A_n^{\mathcal{R}}(d), A_n^{\mathcal{L}}(d))$ is large enough to make the system exhibit spikes, if $d = 1$, there exists only one periodic orbit with period $\delta = \delta(A)$ defined in (3.4). Moreover, all points in $[0, \theta)$ belong to this periodic orbit because of the reset. As a consequence, all initial conditions in $[0, \theta)$ are fixed points of the time-δ return map, and this map is hence the identity.

We now write the conditions for the existence of the fixed point $\bar{x}_n$ in terms of the flow:

$$\varphi(t_n; \bar{x}_n; A) = \theta,$$
$$\varphi(dT - t_n - (n-1)\delta; 0; A) = x',$$
$$\varphi(T - dT; x'; 0) = \bar{x}_n.$$

Clearly, when $d \to 1$, $x' \to \bar{x}_n$ and A tends to a value such that T is a multiple of $\delta(A)$; indeed,

$$n\delta(A)T \to T.$$

As a consequence, for this limiting value of A, the time-T return map, $\mathfrak{s}$, also tends to be the identity in S_n. ∎

3.3. Period adding structures. In this section we study the invariant objects (periodic orbits) located in the regions in the $(d, 1/A)$-parameter space nested in between fixed points of the stroboscopic map (white regions in Figure 1(a)).

As announced in section 2, these are organized by period adding structures. Using the background on this topic provided by Theorem 2.1, this is a direct consequence of the following proposition, which states that the stroboscopic map (3.7) can be written as the normal form given in (2.7) for parameter values between two consecutive regions where fixed points exist.

We recall that Theorem 2.1 needs the piecewise-defined map (2.7) to be contracting in both domains. Lemma 3.4(ii) tells us that this will occur if n is large enough.

Proposition 3.4. *Let*

$$(3.19) \qquad \begin{array}{rccc} \mu : & [0,1] & \longrightarrow & \mathbb{R}^2, \\ & \lambda & \longmapsto & (d(\lambda), B(\lambda)) \end{array}$$

be a C^∞ parametrization of a curve in the $(d, 1/A)$-parameter space such that $\mu(0) = (d_0, B_0)$ and $\mu(1) = (d_1, B_1)$, fulfilling

$$d_i \in (0,1),$$
$$B_0 = \frac{1}{A_n^{\mathcal{L}}(d_0)},$$
$$B_1 = \frac{1}{A_{n+1}^{\mathcal{R}}(d_1)}$$

for some $n > 0$, and

$$B'(\lambda) < 0, \quad \lambda \in (0,1).$$

Let $\mathfrak{s}_\lambda$ be the map obtained by applying the reparametrization μ to $\mathfrak{s}$. Then, if n is large enough, the bifurcation diagram associated with the map $\mathfrak{s}_\lambda$ for $\lambda \in [0,1]$ follows a period adding structure as described for map (2.7).

Proof. We show that the map $\mathfrak{s}$ can be written in the form of map (2.7), fulfilling the conditions of Theorem 2.1.

After performing the reparametrization $\lambda \longmapsto (d, B)$ given by the curve (3.19), we have that $\Sigma_n(\lambda) \in [0, \theta)$ for all $\lambda \in [0,1]$. Hence, the change of variables

$$\tilde{x} \longmapsto x - \Sigma_n(\lambda)$$

is well defined and makes the map $\tilde{\mathfrak{s}}_\lambda(\tilde{x}) := \mathfrak{s}(\tilde{x} + \Sigma_n(\lambda)) - \Sigma_n(\lambda)$ undergo a discontinuity at $\tilde{x} = 0$ independently of λ. Provided that n is large enough and using Lemma 3.4, the stroboscopic map $\tilde{\mathfrak{s}}_\lambda$ is continuous, increasing, and contracting in $[0, \theta - \Sigma_n(\lambda))$ and $[-\Sigma_n(\lambda), 0)$ for $\lambda \in [0,1]$. Hence, the map $\tilde{\mathfrak{s}}_\lambda(\tilde{x})$ is of type (2.7) and satisfies (2.9) in its domain, which is enough, as argued in Remark 2.1.

As argued in the proof of Proposition 3.3, the map $\tilde{\mathfrak{s}}_\lambda(\tilde{x})$ undergoes a negative gap at $\tilde{x} = 0$ for $\lambda \in [0,1]$:

$$(3.20) \qquad \tilde{\mathfrak{s}}_\lambda(0^-) > \tilde{\mathfrak{s}}_\lambda(0^+).$$

For $\lambda = 0$ and $\lambda = 1$, the fixed points $\bar{x}_{n-1} - \Sigma_n(0)$ and $\bar{x}_n - \Sigma_n(1)$ of the map $\tilde{\mathfrak{s}}_\lambda(\tilde{x})$ undergo border collision bifurcations. This implies

$$\tilde{\mathfrak{s}}_0(0^-) = 0,$$
$$\tilde{\mathfrak{s}}_1(0^+) = 0.$$

Hence, condition C.3 of Theorem 2.1 is satisfied. Recalling the negative gap (3.20), the map $\tilde{\mathfrak{s}}_\lambda(\tilde{x})$ fulfills

$$\tilde{\mathfrak{s}}_\lambda(0^+) < 0 \quad \forall \lambda \in (0, 1),$$
$$\tilde{\mathfrak{s}}_\lambda(0^-) > 0 \quad \forall \lambda \in (0, 1),$$

and hence C.1 in Theorem 2.1 is satisfied, too.

From the fact that $B'(\lambda) < 0$, the reparametrization is such that the parameter A monotonically decreases with λ. From Lemma 3.2 we get that $\Sigma_n(\lambda)$ also decreases monotonically with λ, and hence C.2 in Theorem 2.1 is also satisfied.

Finally, we can apply Theorem 2.1 for the normal form map (2.7) to obtain that the bifurcation scenario exhibited by the map $\tilde{\mathfrak{s}}_\lambda$ (and thus by the original map $\mathfrak{s}_\lambda$) when varying λ is given by the period adding structure. ∎

By combining the previous result and the bifurcation scenario described for the normal form map (2.7), we get that the regions in parameter space between curves of the form $(d, 1/A_n^{\mathcal{L}}(d))$ and $(d, 1/A_{n+1}^{\mathcal{R}}(d))$ are covered by an infinite number of periodic orbits with arbitrarily high period following the period adding structure described in section 2. In addition, by combining it with Lemma 3.3, we get the full description of the bifurcation scenario for system (2.1)–(2.3) in the $(d, 1/A)$-parameter space, as described in section 2.

3.4. Symbolic sequences, firing number, and firing rate. We now introduce the symbolic dynamics described in section 2. Let $(x_1, \ldots, x_n)$ be an n-periodic orbit located in the region in parameter space between the curves $(d, 1/A_n^{\mathcal{L}})$ and $(d, 1/A_{n+1}^{\mathcal{R}})$. We then assign to this orbit the symbolic sequence given by the encoding

$$x_i \to \mathcal{L} \quad \text{if } x_i < \Sigma_n,$$
$$x_i \to \mathcal{R} \quad \text{if } x_i \geq \Sigma_n.$$

Note that $x_i < \Sigma_n$ and $x_i \geq \Sigma_n$ correspond to $x_i \in S_{n-1}$ and $x_i \in S_n$, respectively. Hence, recalling the definition of the sets S_i provided in (3.8), when introducing the encoding (2.8), the symbols $\mathcal{L}$ and $\mathcal{R}$ have to be interpreted as the system spiking n and $n + 1$ times for one iteration of the stroboscopic map, respectively. This determines the so-called *firing number*, introduced in [KHR81] as follows.

Definition 3.1. Let s be the total number of spikes performed by a p-periodic orbit of the stroboscopic map $\mathfrak{s}$ when iterated p times, $p \in \mathbb{N}$; then we define the firing number as

(3.21)
$$\eta = \frac{s}{p}.$$

Provided that these periodic orbits are attractive, this number becomes the asymptotic average number of spikes per iteration of the stroboscopic map.

Note that this quantity can be computed from the symbolic sequence. Let σ be a p-periodic orbit for parameter values located between the curves $1/A = 1/A_n^{\mathcal{L}}(d)$ and $1/A = 1/A_{n+1}^{\mathcal{R}}(d)$ whose symbolic sequence contains m $\mathcal{R}'s$ and k $\mathcal{L}'s$ ($k = p - m$). Then, the firing number becomes

$$\eta = \frac{nk + (n+1)m}{p} = n + \frac{m}{p}.$$

As explained in section 2, the rotation numbers associated with the periodic orbits in the period adding structure can be computed by dividing the number of $\mathcal{R}'s$ symbols in its symbolic sequence by its total period,

$$\rho = \frac{m}{p}.$$

Hence, the firing number can be related with the rotation number as

(3.22) $$\eta = n + \rho,$$

where n is such that the periodic orbit steps on each side of the boundary Σ_n.

As also explained in section 2, the rotation number is organized by the Farey tree structure shown in Figure 3(a) when parameters are varied from the bifurcation curve $1/A = 1/A_n^{\mathcal{L}}(d)$ toward $1/A = 1/A_{n+1}^{\mathcal{R}}(d)$ along curves such as that given in Proposition 3.4. Hence, it follows a devil's staircase from 0 to 1. As a consequence, the firing number follows a devil's staircase from n to $n + 1$ when parameters d and A are varied as mentioned.

Taking into account that the stroboscopic map consists of flowing system (2.1)–(2.3) for a time T, the firing number allows one to compute the *firing rate* associated with the corresponding periodic orbit as

$$r = \frac{\eta}{T}.$$

This becomes the asymptotic number of spikes per unit time.

Note that, provided that these periodic orbits are attracting, r becomes the asymptotic firing rate defined in (2.6),

$$r = \lim_{\tau \to \infty} \frac{\#(\text{spikes performed by } \phi(t; x_0) \text{ for } t \in [0, \tau])}{\tau},$$

which does not depend on $x_0 \in [0, \theta)$.

Using the relation given in (3.22), the firing rate also follows a devil's staircase from n/T to $(n+1)/T$ when the parameter values are varied through curves such as that in Proposition 3.4 between the bifurcation curves $1/A = 1/A_n^{\mathcal{L}}(d)$ and $1/A = 1/A_{n+1}^{\mathcal{R}}(d)$, respectively.

4. Examples. In this section we illustrate the results presented so far in two different examples. We consider a system of the type

$$\dot{x} = f(x) + I(t),$$

with $I(t)$ a T-periodic input as defined in (2.2) and three different types of functions for $f(x)$ satisfying conditions H.1–H.2. The first example consists of a linear system, leading to the so-called *linear integrate-and-fire* system:

(4.1) $$f_1(x) = ax + b.$$
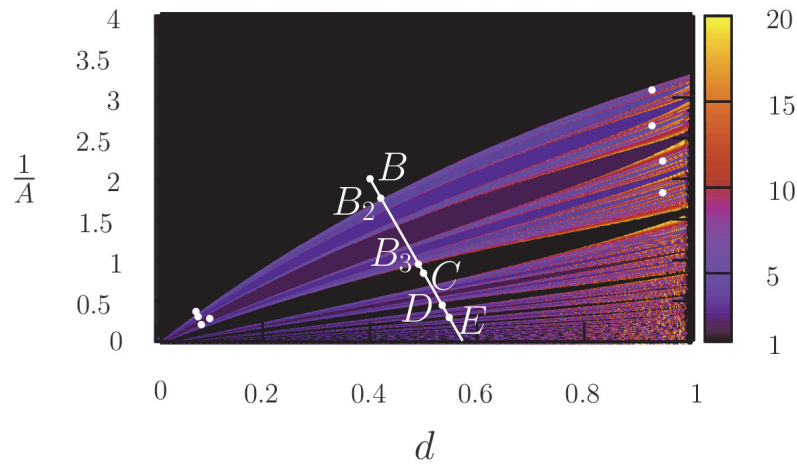
**Figure 7.** *Bifurcation diagram for the map* $\mathfrak{s}$ *for* $T = 1.9$, $a = -0.5$, $b = 0.2$ *associated with system* (2.1)–(2.3) *for the linear system* (4.1)*. The colors refer to the periods of the periodic orbits found by simulating the system. Periodic orbits are shown only up to period* 20 *for clarity reasons. The* T-*periodic orbits (fixed points of* $\mathfrak{s}$*) for parameter values corresponding to points* B *and* C*, as well as their bifurcations (*B_2 *and* B_3*), are shown in Figure* 9*. The eight nonlabeled points correspond to* $5T$-*periodic orbits with four different symbolic sequences. Those for the four points with small values of* d *are shown in Figure* 10*, and those with large values of* d *are shown in Figure* 11*.*
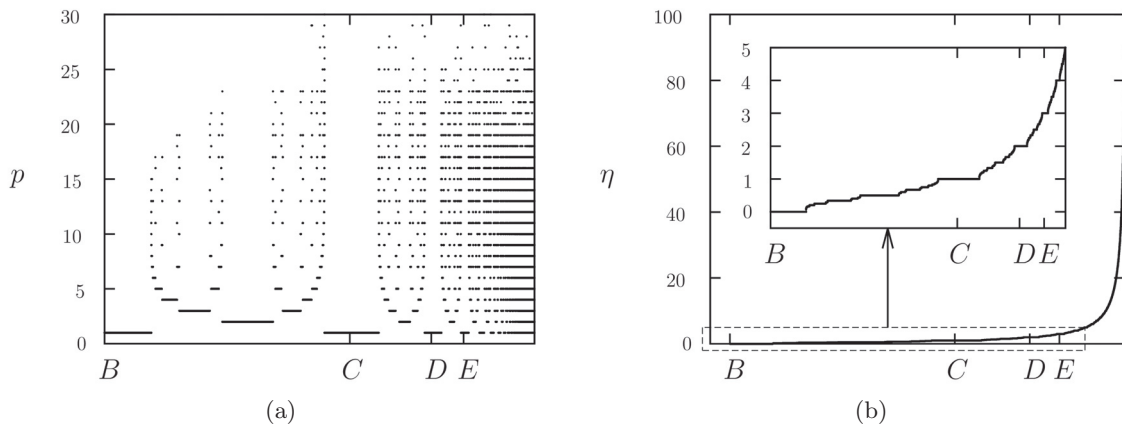
Figure 8. (a) *Periods of the periodic orbits found along a line such as that shown in Figure* 7*.* (b) *Firing number associated with such periodic orbits.*

Taking the threshold $\theta = 1$, conditions H.1–H.2 are satisfied if $a < 0$ and $-b/a \in (0, 1)$. In Figure 7 we show the existence of periodic orbits in the $(d, 1/A)$-parameter space, which is as predicted. In Figure 8(a) we show the periods of the periodic orbits found along the line drawn in Figure 7, although the bifurcation scenario is topologically the same for any other curve
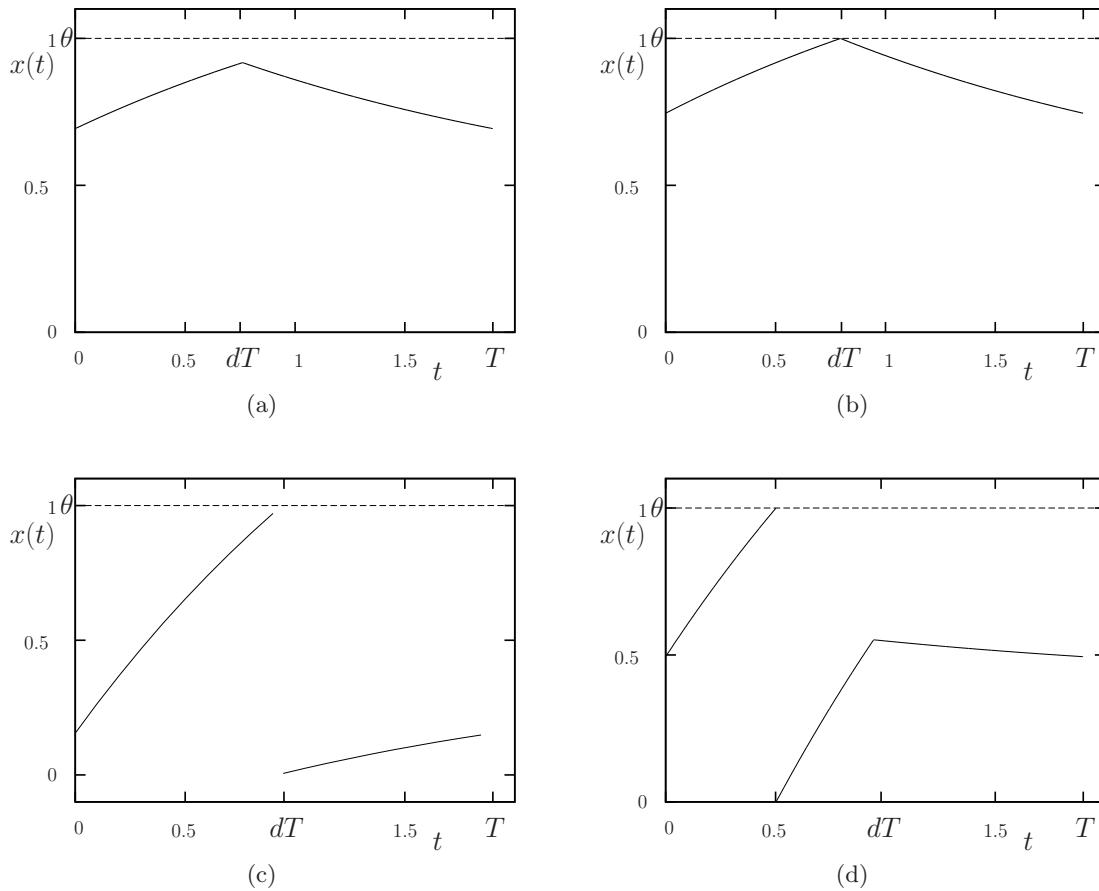
Figure 9. *Periodic orbits for the labeled points in Figure* 7. (a) *Periodic orbit with no spikes (fixed point* $\bar{x}_0$); (b) *left bifurcation of the fixed point,* $\bar{x}_0 = \Sigma_1$; (c) *right bifurcation of the fixed point,* $\bar{x}_1 = \Sigma_1$; (d) *periodic orbit spiking once.*

transversally crossing the colored regions. As one can see in Figure 8(a), along such a curve there exist regions where one finds only T-periodic orbits (fixed points of the stroboscopic map, period 1). These are the black regions in Figure 7, for example containing the points as B, C, D, and E. The periodic orbits for the parameter values corresponding to B and C are shown in Figures 9(a) and 9(d), respectively. Note that their associated firing number defined in (3.22) (average number of spikes per iteration of the stroboscopic map) is 0 and 1, respectively.

As given by Propositions 3.2 and 3.3, there exists an infinite number of regions, accumulating at the horizontal axis $1/A = 0$, for which one finds T-periodic orbits with arbitrarily large integer firing numbers. This can be seen in Figure 8(b) for the points D and E and successive regions containing T-periodic orbits (period one Figure 8(a)). As one can see in Figure 8(a), the period adding between the points B and C is not complete, as there are some periodic orbits "missing." This is due to the fact that, for the chosen parameter values,
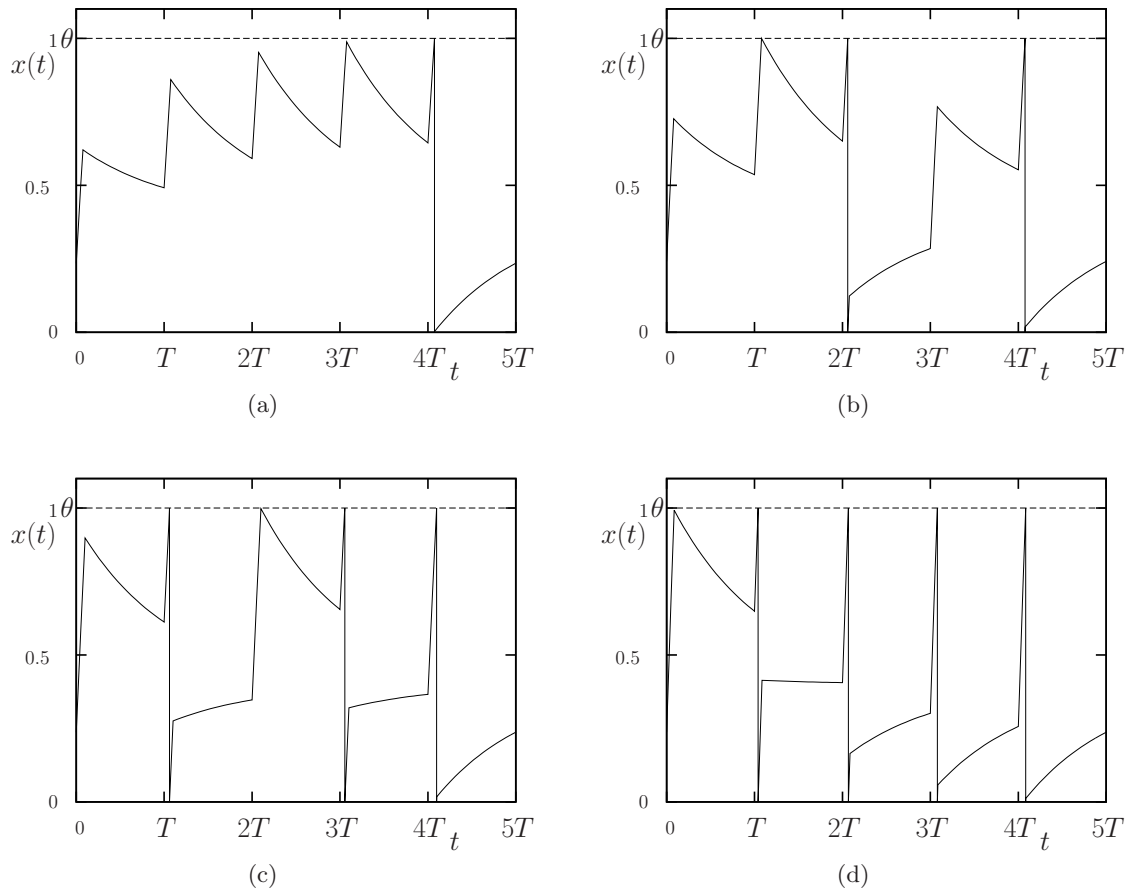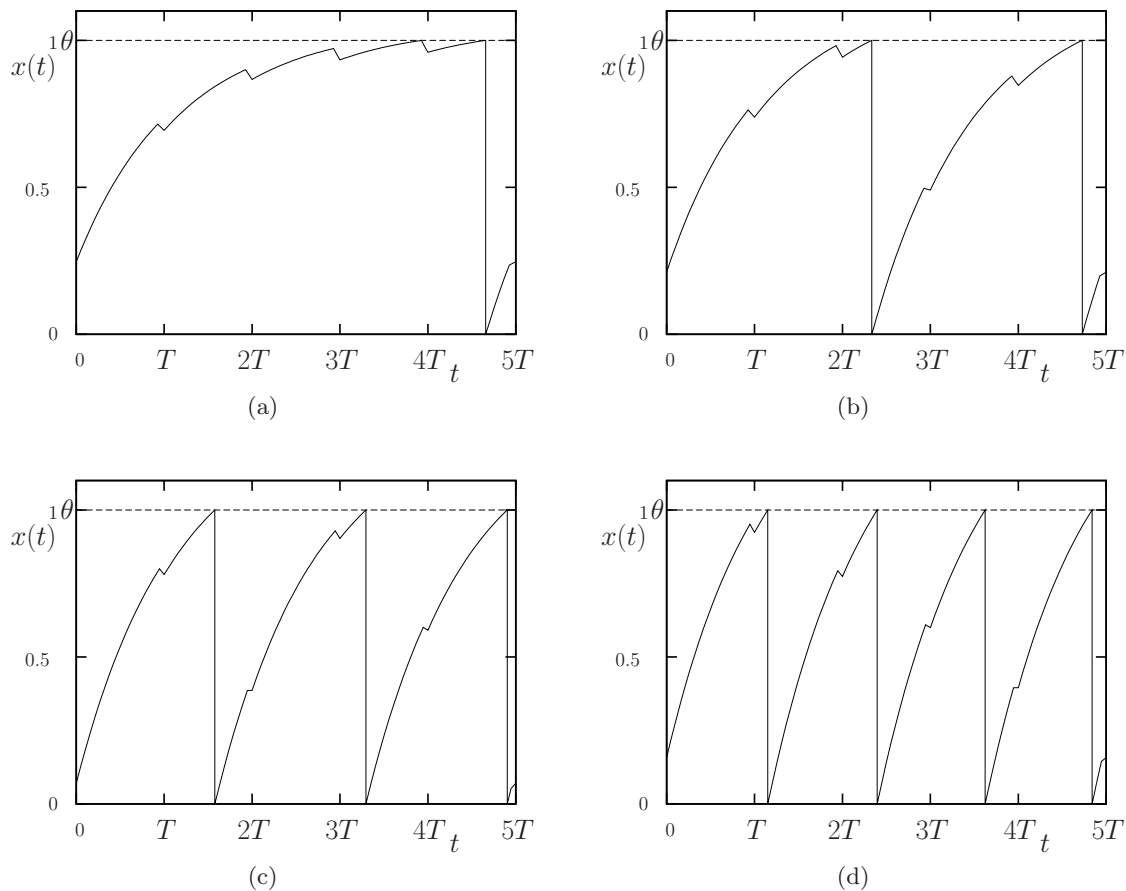
Figure 10. *Period-5 periodic orbits with different symbolic sequences and firing number: $\mathcal{L}^4\mathcal{R}$ $\eta = 1/5$ (a), $\mathcal{L}^2\mathcal{R}\mathcal{L}\mathcal{R}$ $\eta = 2/5$ (b), $\mathcal{L}\mathcal{R}\mathcal{L}\mathcal{R}^2$ $\eta = 3/5$ (c), and $\mathcal{L}\mathcal{R}^4$ $\eta = 4/5$ (d). Parameter values for which these periodic orbits exist are marked with points in Figure 7 and correspond to small values of the duty cycle d.*

the map $\mathfrak{s}$ is not contracting in $[\Sigma_1, \theta)$, and hence these periodic orbits are not unique and unstable (see [GAK14]). However, as stated in Lemma 3.4, when A (or equivalently n) is large enough, $\mathfrak{s}$ becomes contracting, and the period adding is complete as these parameters are further varied along the curve shown in Figure 7.

The two T-periodic orbits found in B and C undergo border collision bifurcations at the points B_2 and B_3 labeled in Figure 7. The periodic orbits at the moment of the bifurcation are shown in Figures 9(b) and 9(c), respectively. This occurs similarly for all other T-periodic orbits with higher firing number (see Proposition 3.3 for more details). In between points B and C, C and D, D and E, etc., a period adding bifurcation occurs; that is, there exists an infinite number of periodic orbits whose periods, symbolic sequences, and rotation numbers are organized by the Farey tree structure shown in Figure 3(a). After applying the symbolic encoding (2.8), the symbolic sequences and periods are obtained by successive concatenation and addition, as shown in Figure 3(a) and explained in section 2. In Figures 10 and 11 we

Figure 11. *Period 5 periodic orbits with different symbolic sequences and firing number: $\mathcal{L}^4\mathcal{R}$ $\eta = 1/5$ (a), $\mathcal{L}^2\mathcal{R}\mathcal{L}\mathcal{R}$ $\eta = 2/5$ (b), $\mathcal{L}\mathcal{R}\mathcal{L}\mathcal{R}^2$ $\eta = 3/5$ (c), and $\mathcal{L}\mathcal{R}^4$ $\eta = 4/5$ (d). Parameter values for which these periodic orbits exist are marked with points in Figure 7 and correspond to large values of the duty cycle d.*

show, for different parameter values, the four periodic orbits with period 5 located in the adding structure between points B and C, which correspond to the symbolic sequences $\mathcal{L}^4\mathcal{R}$, $\mathcal{L}^2\mathcal{R}\mathcal{L}\mathcal{R}$, $\mathcal{L}\mathcal{R}\mathcal{L}\mathcal{R}^2$, and $\mathcal{L}\mathcal{R}^4$ (see the Farey tree in Figure 3(a)). The parameter values used are given by the points marked in Figure 7 for large and small d. Note how the $\mathcal{L}$ symbol corresponds to an iteration of the stroboscopic map without exhibiting any spike, whereas for $\mathcal{R}$ one spike occurs.

The firing number associated with the periodic orbits is related to their rotation number through (3.22), and it is shown in Figure 8(b) for the periodic orbits found along the line labeled in Figure 7. According to Proposition 3.4 (see section 3.4), the firing number is a strictly increasing and unbounded devil's staircase as a function of the parameters.

Finally, we show that the same results apply for system (2.1)–(2.3) with $f(x)$ not necessarily linear as long as conditions H.1–H.2 are satisfied. To illustrate this we choose two
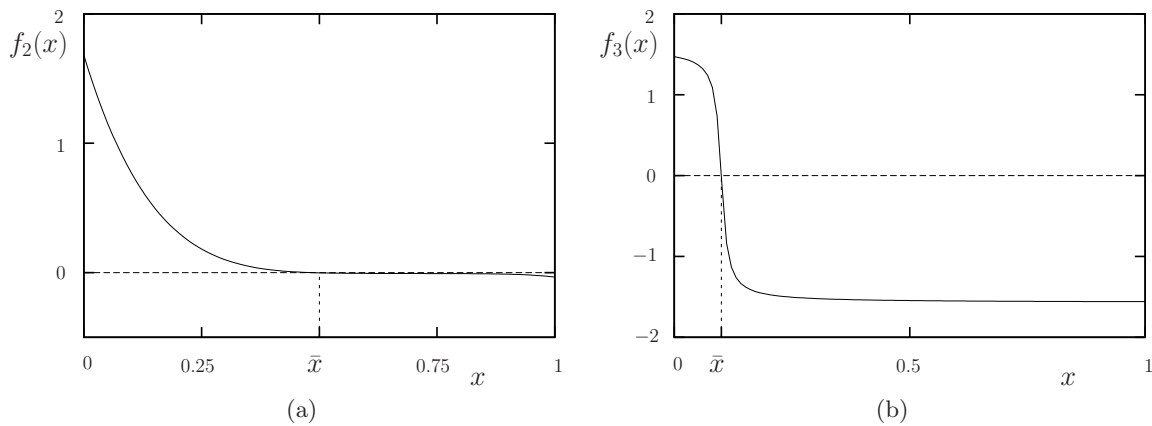
Figure 12. *Functions f_2 and f_3 given in* (4.2). *$\bar{x}$ is the attracting equilibrium point.*

different functions for f:

$$(4.2) \qquad \begin{aligned} f_2(x) &= a_2 \, (x - b_2)^5 - c_2 x, \\ f_3(x) &= - \arctan(a_3(x - b_3)). \end{aligned}$$

With $\theta = 1$, we choose parameter values in order to make the functions f_2 and f_3 satisfy conditions H.1–H.2:

$$\begin{aligned} a_2 &= -10, \\ b_2 &= 0.7, \\ c_2 &= 0.01, \end{aligned} \qquad \begin{aligned} a_3 &= 100, \\ b_3 &= 0.1. \end{aligned}$$

These two functions are shown for these parameter values in Figure 12. One can see that the first case corresponds to a weak equilibrium point, whereas the second corresponds to a robust one. This leads to slow and fast subthreshold dynamics, respectively.

The bifurcation structures in the $(d, 1/A)$-parameter space, shown in Figure 13, are as predicted. The bifurcation scenarios along curves transversally crossing the bifurcation curves are equivalent to those for the first example, as predicted by our results, and we do not show further details.

The bifurcation scenario in the $(d, 1/A)$-parameter space for the weak equilibrium point is mainly covered by periodic orbits (bursting spiking), whereas in the second case, the spiking dynamics is mainly given by fixed points of the stroboscopic map (tonic spiking). This is because the subthreshold dynamics for f_2 is much slower than for f_3. This can be seen in Figure 14, where we show for both systems a 5-periodic orbit with symbolic sequence $\mathcal{LRLR}^2$. Note that the value of T for f_3 in Figure 13(b) had to be reduced with respect to Figure 13(a) in order to observe bursting spiking (periodic orbits) because, due to the fast subthreshold dynamics, for the same value of T as for f_2 one basically observes tonic spiking (fixed points). When reducing the period, the fast convergence of the subthreshold dynamics for f_3 is compensated, and hence the regions in parameter space locating fixed points become

(a)

(b)
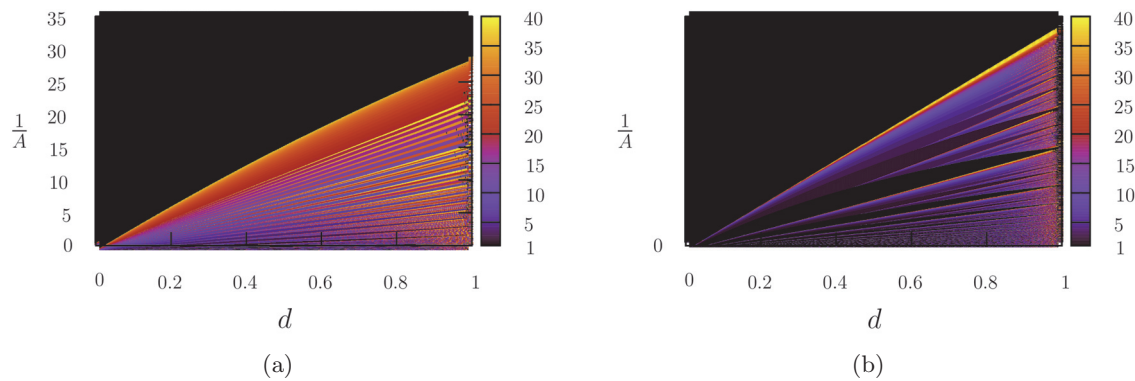
Figure 13. *Bifurcation scenarios for the second and third examples given in* (4.2). *(a) and (b) correspond to f_2 and f_3, respectively. The values of the period T have been $T = 1$ for (a) and $T = 0.5$ for (b).*

(a)

(b)
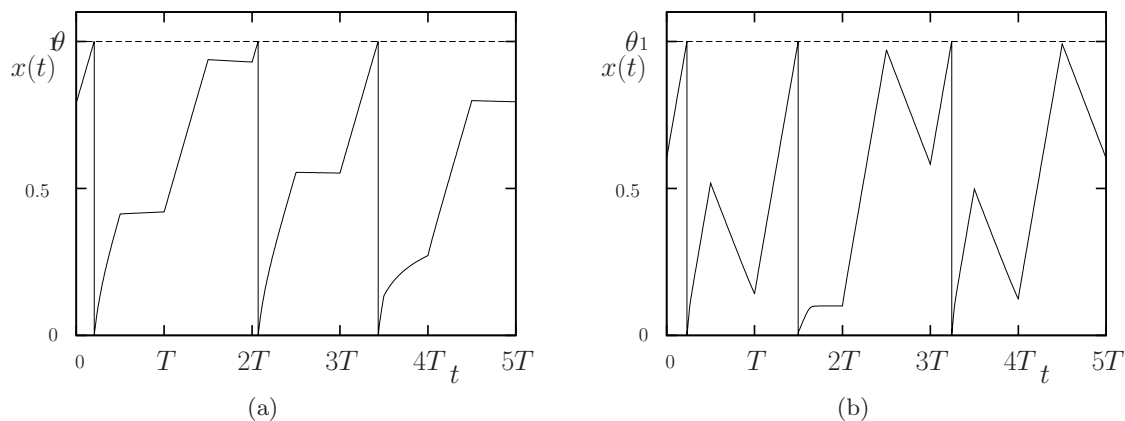
Figure 14. *Period-5 periodic orbits with symbolic sequence $\mathcal{LRLR}^2$ and firing number $\eta = 3/5$ for the examples given in* (4.2). *(a) corresponds to f_2 and (b) to f_3. Parameter values are $1/A = 0.79$ and $1/A = 0.2$ for (a) and (b), respectively, and $d = 0.5$ in both cases.*

broader and more easily observable. We refer the reader to [GK14] for a complete study of the behavior of the bifurcation curves under frequency variation of the input.

5. Discussion. Hybrid systems with resets are a simplified version of excitable systems and are widely used in the modeling of biological systems, e.g., in the context of neuronal activity and secretion of hormones. Typically, as such systems undergo discontinuities (spikes), they are studied by means of firing maps, or impact maps, i.e., Poincaré maps defined using the threshold as a Poincaré section. In this work we have studied generic periodically forced hybrid systems under the assumption of monotonicity and contracting dynamics. The main innovation of this paper was to use the stroboscopic (time-T return map) rather than the return map. We have obtained a complete description of the bifurcation structure underlying

the dynamics, showing the existence of a globally attracting periodic orbit for every parameter value as well as giving a description of the transitions between different regions of stable periodicity. We have also introduced the rotation number and shown that its typical dependence on parameters is a devil's staircase. Finally, we defined the firing rate in the context of these systems and related it to the rotation number.

It is important and interesting to compare the method developed in this paper with the approach based on the firing map. The main reason the firing map has been the tool of choice is that in certain contexts it becomes a regular map; however, the analysis relies on explicit computation of the firing times, and hence this method may not be suitable to provide general results that can be systematically applied. Firing maps become even more difficult to use in the presence of time dependent periodic forcings, as one needs to check for congruency between spiking times and the period of the forcing.

The property of smoothness, which is the main advantage of the firing map, holds automatically for systems in one dimension, as the threshold is a real number which is identified with a different real number by means of the reset. However, in higher dimensions (when considering dynamical adaptation currents or dynamical thresholds), the threshold becomes a codimension-one manifold, and one can find much richer dynamics. In fact, the firing map may exhibit discontinuities near those points where the flow exhibits tangencies with the threshold. As shown in [CTW12, JMB$^+$13] for two-dimensional linear systems that can be solved explicitly, the firing map may exhibit opposite slopes on both sides of such discontinuities. In this case, one can apply the results for piecewise-smooth maps given in [AGS11] to obtain a full description of the *bursting* spiking dynamics (periodic orbits of the map) and its symbolic dynamics.

The advantage of using the stroboscopic map when considering periodically forced systems with resets is that, after proper reparametrizations, it can be classified as a discontinuous map with positive slopes near the discontinuity. Such maps have been extensively studied and are well understood [CGT84, GGT84, GIT84, GPTT86, Gam87, PTT87, TS86, GGT88, GT88, LPZ89, AS06] (see [GAK14] for a review). This allows us to provide general results that can be systematically applied to systems satisfying generic conditions. Moreover, the whole analysis of the period adding bifurcation structures comes from understanding only the bifurcations undergone by fixed points and is independent of the number of spikes exhibited by the periodic orbits corresponding to these fixed points for the time continuous system. Finally, the presented framework is well suited for generalizations of the considered systems. For example, a similar analysis can be done for general periodic forcings, systems with expansive subthreshold dynamics, or even systems in higher dimensions, as could be the case when considering a dynamical threshold.

REFERENCES

[AGS11]   V. Avrutin, A. Granados, and M. Schanz, *Sufficient conditions for a period increment big bang bifurcation in one-dimensional maps*, Nonlinearity, 24 (2011), pp. 2575–2598.

[AS06]   V. Avrutin and M. Schanz, *On multi-parametric bifurcations in a scalar piecewise-linear map*, Nonlinearity, 19 (2006), pp. 531–552.

[BG05]   R. Brette and W. Gerstner, *Adaptive exponential integrate-and-fire model as an effective description of neuronal activity*, J. Neurophysiol., 94 (2005), pp. 3637–3642.

[BM61]   N.N. Bogoliubov and Y.A. Mitropolski, *Asymptotic Methods in the Theory of Non-linear Oscillations*, Gordon and Breach, New York, 1961.

[CB99]   S. Coombes and P.C. Bressloff, *Mode locking and Arnold tongues in integrate-and-fire neural oscillators*, Phys. Rev. E, 60 (1999), pp. 2086–2096.

[CGT84]   P.C. Coullet, J.M. Gambaudo, and C. Tresser, *Une nouvelle bifurcation de codimension 2: Le colage de cycles*, C. R. Acad. Sci. Paris Ser. I Math., 299 (1984), pp. 253–256.

[COS01]   S. Coombes, M. Owen, and G.D. Smith, *Mode locking in a periodically forced integrate-and-fire-or-burst neuron model*, Phys. Rev. E, 64 (2001), 041914.

[CPF08]   J.R. Clay, D. Paydarfar, and D.B. Forger, *A simple modification of the Hodgkin and Huxley equations explains type 3 excitability in squid giant axons*, J. R. Soc. Interface, 5 (2008), pp. 1421–1428.

[CTW12]   S. Coombes, R. Thul, and K.C.A. Wedgwood, *Nonsmooth dynamics in spiking neuron models*, Phys. D, 241 (2012), pp. 2042–2057.

[dBBCK08]   M. di Bernardo, C.J. Budd, A.R. Champneys, and P. Kowalczyk, *Piecewise-Smooth Dynamical Systems: Theory and Applications*, Appl. Math. Sci. 163, Springer, New York, 2008.

[DKTG12]   M. Dipoppa, M. Krupa, A. Torcini, and B.S. Gutkin, *Splay states in finite pulse-coupled networks of excitable neurons*, SIAM J. Appl. Dyn. Syst., 11 (2012), pp. 864–894.

[Fit61]   R. FitzHugh, *Impulses and physiological states in models of nerve membrane*, Biophys. J., 1 (1961), pp. 445–466.

[GAK14]   A. Granados, Ll. Alsedà, and M. Krupa, *Period Adding and Incrementing Gluing Bifurcations in One-Dimensional Piecewise-Smooth Maps: Theory and Applications*, preprint, http://arxiv.org/abs/1407.1895 (2014).

[Gam87]   J.M. Gambaudo, *Ordre, désordre, et frontiére des systèmes Morse-Smale*, Ph.D. thesis, Université de Nice, Nice, France, 1987.

[GGT84]   J.M. Gambaudo, P. Glendinning, and C. Tresser, *Collage de cycles et suites de Farey*, C. R. Acad. Sci. Paris Ser. I Math., 299 (1984), pp. 711–714.

[GGT88]   J.M. Gambaudo, P. Glendinning, and T. Tresser, *The gluing bifurcation: Symbolic dynamics of the closed curves*, Nonlinearity, 1 (1988), pp. 203–214.

[GH83]   J. Guckenheimer and P.J. Holmes, *Nonlinear Oscillations, Dynamical Systems and Bifurcations of Vector Fields*, Appl. Math. Sci. 42, Springer, New York, 1983.

[GIT84]   J.M. Gambaudo, O. Lanford, III, and C. Tresser, *Dynamique symbolique des rotations*, C. R. Acad. Sci. Paris Ser. I Math., 299 (1984), pp. 823–826.

[GK14]   A. Granados and M. Krupa, *Firing-Rate, Symbolic Dynamics and Frequency Dependence in Periodically Driven Spiking Models: A Piecewise-Smooth Approach*, preprint, http://arxiv.org/abs/1310.1216 (2014).

[GPTT86]   J.M. Gambaudo, I. Procaccia, S. Thomae, and C. Tresser, *New universal scenarios for the onset of chaos in Lorenz-type flows*, Phys. Rev. Lett., 57 (1986), pp. 925–928.

[GT88]   J. Gambaudo and C. Tresser, *On the dynamics of quasi-contractions*, Bol. Soc. Bras. Mat., 19 (1988), pp. 61–114.

[HH52]   A.L. Hodgkin and A.F. Huxley, *A quantitative description of membrane current and its application to conduction and excitation in nerve*, J. Physiol., 117 (1952), pp. 500–544.

[Izh03]   E.M. Izhikevich, *Simple model of spiking neurons*, IEEE Trans. Neur. Networks, 6 (2003), pp. 1569–1572.

[Izh07]   E.M. Izhikevich, *Dynamical Systems in Neuroscience: The Geometry of Excitability and Bursting*, Computational Neuroscience, MIT Press, Cambridge, MA, 2007.

[JMB+13]   N.D. Jimenez, S. Mihalas, R. Brown, E. Niebur, and J. Rubin, *Locally contractive dynamics in generalized integrate-and-fire neurons*, SIAM J. Appl. Dyn. Syst., 12 (2013), pp. 1474–1514.

[KHR81]   J.P. Keener, F.C. Hoppensteadt, and J. Rinzel, *Integrate-and-fire models of nerve mem-brane response to oscillatory input*, SIAM J. Appl. Math., 41 (1981), pp. 503–517.

[LPZ89]   D.V. Lyubimov, A.S. Pikovsky, and M.A. Zaks, *Universal Scenarios of Transitions to Chaos via Homoclinic Bifurcations*, Math. Phys. Rev. 8, Harwood Academic, London, 1989. Russian version: Preprint 192 of Russian Academy of Science, Institute of Mechanics of Solid Matter, Sverdlovsk, Russia, 1986.

[MHR12]   X. Meng, G. Huguet, and J. Rinzel, *Type* III *excitability, slope sensitivity and coincidence detection*, Discrete Contin. Dyn. Syst., 32 (2012), pp. 2720–2757.

[ML81]   L. Morris and H. Lecar, *Voltage oscillations in the barnacle giant muscle fiber*, J. Biophys., 35 (1981), pp. 193–213.

[NAY62]   J. Nagumo, S. Arimoto, and S. Yoshizawa, *An active pulse transmission line simulating nerve axon*, Proc. IRE, 50 (1962), pp. 2061–2070.

[PTT87]   I. Procaccia, S. Thomae, and C. Tresser, *First-return maps as a unified renormalization scheme for dynamical systems*, Phys. Rev. A, 35 (1987), pp. 1884–1900.

[TB09]   J. Touboul and R. Brette, *Spiking dynamics of bidimensional integrate-and-fire neurons*, SIAM J. Appl. Dyn. Syst., 8 (2009), pp. 1462–1506.

[TS86]   D.V. Turaev and L.P. Shil'nikov, *On bifurcations of a homoclinic "Figure of Eight" for a saddle with a negative saddle value*, Soviet Math. Dokl., 34 (1987), pp. 397–401 (translation of the 1986 Russian version).